Evolution of nuclear structure in the neutron-rich ^{96,97,99}Nb isotopes: Evidence for shape coexistence in $N = 58$ ^{99}Nb

V. Kumar,[1,2,*] R. Chapman,[1,2,†] D. O'Donnell,[1,2] J. Ollier,[1,2,‡] R. Orlandi,[3] J. F. Smith,[1,2] K.-M. Spohr,[1,2,§] D. A. Torres,[1,2,‖] P. Wady,[1,2,¶] S. K. Tandel,[4] S. J. Freeman,[5,**] G. de Angelis,[6] N. Mărginean,[6,††] D. R. Napoli,[6] J. J. Valiente-Dobón,[6] S. Aydin,[7,‡‡] E. Farnea,[7,§§] R. Mărginean,[7,††] D. Mengoni,[7] T. Kröll,[7,‖‖] and N. Thompson[8]

[1]*School of Computing, Engineering, and Physical Sciences, University of the West of Scotland, Paisley PA1 2BE, United Kingdom*

[2]*The Scottish Universities Physics Alliance (SUPA), United Kingdom*

[3]*Advanced Science Research Center, Japan Atomic Energy Agency, Tokai, Ibaraki 319-1195, Japan*

[4]*Department of Physics, School of Natural Sciences, Shiv Nadar Institution of Eminence, Gautam Buddha Nagar 201314, India*

[5]*Schuster Laboratory, University of Manchester, Manchester M13 9PL, United Kingdom*

[6]*INFN-Laboratori Nazionali di Legnaro, I-35020 Legnaro (Padova), Italy*

[7]*INFN Sezione di Padova and Dipartimento di Fisica dell'Università, I-35131 Padova, Italy*

[8]*School of Mathematics and Physics, University of Surrey, Guildford GU2 7XH, United Kingdom*

(Received 22 May 2023; accepted 22 September 2023; published 19 October 2023)

Excited states of the neutron-rich niobium isotopes $^{96,97,98,99}_{41}$Nb have been populated in two experiments which used fusion-fission and multinucleon binary grazing reactions to populate high-spin yrast states. In the multinucleon-transfer experiment, a 530-MeV beam of ^{96}Zr ions was incident on a thin ^{124}Sn target; projectile-like ejectiles were detected and identified using the PRISMA magnetic spectrometer and the associated γ rays were detected using the CLARA array of Ge detectors. In the second experiment, the GASP array of escape-suppressed Ge detectors was used to detect γ rays from fusion-fission products formed following the interaction of a 230-MeV beam of ^{36}S ions with a thick target of ^{176}Yb. Level schemes of ^{96,97,99}Nb were established up to excitation energies of 4545, 5409, and 3814 keV, respectively; states with proposed spin values up to about 15 $\hbar$ were populated. Gamma-ray photopeaks corresponding to transitions in ^{98}Nb were also observed in the PRISMA-CLARA experiment; however, it was not possible, in this case, to produce a level scheme based on γ-ray coincidence data from the GASP experiment. For ^{96}Nb and ^{97}Nb, the level schemes are in agreement with the results of earlier publications. Two new decay sequences have been populated in ^{99}Nb; tentative J^{π} values of the hitherto unobserved states have been assigned through comparisons with J^{π} values of neighboring nuclei. In contrast with earlier published studies of the high-spin spectroscopy of ^{96}Nb and ^{97}Nb, the present work provides an unambiguous association of the observed γ rays with the A and Z of the excited nucleus. The structure of the yrast states of ^{96,97,99}Nb is discussed within the context of shell-model calculations. The experimental results, supported by model calculations, indicate the first observation of shape coexistence at low spin and low excitation energy in the $N = 58$ nucleus ^{99}Nb. The results of TRS calculations indicate that the

*Present address: Department of Physics, University of Lucknow, Lucknow 226007, India; vinod2.k2@gmail.com

†Robert.Chapman@uws.ac.uk

‡Present address: Rapiscan Systems, Prospect Way, Victoria Business Park, Biddulph, Stoke-on-Trent ST8 7PL, United Kingdom.

§Present address: Extreme Light Infrastructure (ELI-NP) & IFIN-HH, Horia Hulubei National Institute of Physics and Nuclear Engineering, Bucharest-Măgurele RO-077125, Romania.

‖Present address: Departamento de Física, Universidad Nacional de Colombia, Bogotá, Colombia.

¶Present address: Diamond Light Source Ltd., Diamond House, Harwell Science & Innovation Campus, Didcot OX11 0DE, United Kingdom.

**Present address: EP Department, CERN, Geneva CH-1211, Switzerland.

††Present address: IFIN-HH, Horia Hulubei National Institute of Physics and Nuclear Engineering, Bucharest-Măgurele RO-077125, Romania.

‡‡Present address: Department of Natural and Mathematical Sciences, Faculty of Engineering, Tarsus University, 33480 Mersin, Turkey.

§§Deceased.

‖‖Present address: Institut für Kernphysik, Technische Universität Darmstadt, 64289 Darmstadt, Germany.

$9/2^+$ ground state is triaxial, tending to oblate shapes with a transition to a more deformed prolate shape beyond the $17/2^+$ member of the decay sequence; here the sequence has been observed to $(29/2^+)$. On the other hand, the previously unobserved decay sequence based on the $5/2^-$ state at 631 keV exhibits the characteristics of a rotational sequence and has been assigned Nilsson quantum numbers $5/2^-[303]$. TRS calculations indicate that the $5/2^-[303]$ band is gamma soft and this is consistent with the inability of the particle-rotor model to reproduce the observed behavior of the signature-splitting function.

DOI: 10.1103/PhysRevC.108.044313

I. INTRODUCTION

Nuclei with "magic numbers" of nucleons have spherical ground states. Moving away from magicity, the polarizing effect of added nucleons leads to deformation. Throughout the nuclear landscape, the onset of deformation is usually a gradual process; however, in neutron-rich nuclei around mass $A \approx 100$, the shape change is rather sudden as indicated by 2^+ and 4^+ level energy systematics and enhanced $B(E2)$ values [1]. The abrupt change in ground-state deformation occurs exactly at $N = 60$ for a number of elements, namely Rb, Sr, Y, and Zr. The $N = 58$ isotones are spherical while those with $N = 60$ are highly deformed. For elements with $Z < 37$ and for those with $Z > 40$, the change in deformation is more gradual. Deformations are as large as $\beta_2 = 0.40$ for $^{98}_{38}$Sr and $^{99}_{39}$Y [2,3], while they reduce slightly with increasing Z [4–7]; additionally, triaxiality also becomes evident. A shape transition from axially symmetric in Zr ($Z = 40$) to triaxial in Mo ($Z = 42$) isotopes [8] was identified in even-Z nuclei. For the ground-state bands of odd-Z nuclei with Z in the range from 39 to 45, the nuclear shape changes from axial symmetry for Y ($Z = 39$) to near maximum triaxiality for Rh ($Z = 43$) [9]. Further, with increasing Z, the triaxial deformation increases while the quadrupole deformation decreases [9]. Such a correlation of quadrupole deformation and triaxiality is generally known; it has been examined in quantitative terms in Ref. [10]. The present spectroscopic information on the Nb ($Z = 41$) isotopes may allow searches for the expected triaxial shape transition in the odd-Z nuclei in this important region.

Nuclear structure in this region is generally understood in terms of single-particle excitations across shell and subshell closures at $Z = 38$, 40 and $N = 50$, 56. The behavior as a function of proton number is related to the vanishing of the $d_{5/2}$ neutron subshell closure. There are, however, some nuclei in this region which have not been well studied at higher spin. The isotopes studied in this work, ^{96,97,99}Nb are on the neutron-rich side of the stability line, namely three, four, and six neutrons, respectively, from the stable isotope, ^{93}Nb, and are not readily populated in reactions that bring in significant angular momentum, such as fusion-evaporation reactions with stable beam-target combinations. They can, however, be populated in binary grazing reactions and in fusion-fission processes. Indeed, states of ^{96}Nb and of ^{97}Nb have been populated in fusion-fission reactions with accelerated beams of ^{24}Mg and ^{23}Na, which resulted in the first study of the high-spin level structures of both isotopes [11]. No high-spin studies of ^{99}Nb have, to date, been reported in the literature.

The objective of the present work is to study the spectroscopic properties of odd-Z isotopes in the $A \approx 100$ region and, in particular, of the neutron-rich niobium isotopes. The study of high-spin states in ^{96,97,99}Nb provides new information important for an understanding of the coupling of nucleons to the subshell closure which occurs in ^{96}Zr. The spectroscopic information that exists for these nuclei is summarized in Refs. [12–17] and originates from nucleon pick-up reactions and β decay. A preliminary report on the high-spin states of ^{96,97,99}Nb from the present work was presented in Ref. [18]. More recently, a spectroscopic study of high-spin states of ^{96,97}Nb through the study of γ rays from two fusion-fission reactions was reported by Fotiades *et al.* [11]. A comparison between the experimental yrast level structure and the results of shell-model calculations is presented. The role of the gamma degree of freedom in the observed signature splitting in the $5/2^-[303]$ bands of ^{99}Nb, ^{101}Nb, and ^{103}Nb is examined through comparison with the results of particle-rotor-model calculations. Cranking calculations have also been performed using the Ultimate Cranker (UC) code [19]. The calculations, which support experimental observation, indicate the presence of shape coexistence at low spin and low excitation energy in ^{99}Nb. While γ-ray photopeaks corresponding to transitions in ^{98}Nb have been identified in the PRISMA-CLARA experiment, it did not prove possible to establish a level scheme based on the data from the GASP experiment.

II. EXPERIMENTAL METHODS AND RESULTS

The neutron-rich nuclei ^{96,97,98,99}Nb were produced at high spin in two experiments employing fusion-fission and binary grazing reactions; the fusion-fission reaction was initiated following the interaction of ^{36}S ions at 230 MeV with a ^{176}Yb target, while the binary grazing reaction was initiated through the interaction of ^{96}Zr ions at 530 MeV with a ^{124}Sn target. The combined XTU-Tandem Van de Graaff and ALPI accelerators at the INFN Legnaro National Laboratory, Italy, were used to deliver the beams on target. In the first experiment, the compound nucleus formed in the fusion-fission reaction at high spin and excitation energy was ^{212}Rn. A 14-mg cm^{-2} target of ^{176}Yb, isotopically enriched to 97.8%, was used with an isotopically enriched ^{208}Pb (98.7%) backing of thickness 35 mg cm^{-2} to stop forward-moving recoiling nuclei. Prompt γ rays from fission fragments were detected with the GASP array [20,21] consisting of 40 escape suppressed HpGe detectors. Data were recorded in an event-by-event mode with a trigger condition of three or more Ge detector signals observed in prompt coincidence; 5.9 billion coincidence events were collected. In the second experiment, a

300-μg cm^{-2} target of ^{124}Sn, enriched to 94.6%, with a carbon backing of thickness 40 μg cm^{-2}, was used. Projectile-like species produced via multinucleon binary grazing reactions were detected and identified using the PRISMA magnetic spectrometer [22,23], in coincidence with their associated deexcitation γ rays detected by the CLARA Ge array of escape-suppressed Ge detectors [24]. Ion tracking through the magnetic spectrometer together with time-of-flight measurements were used to determine the velocity vector of the projectile-like fragments. This allowed appropriate Doppler corrections of γ-ray energies to be performed on an event-by-event basis [25].

PRISMA [22] is a large-acceptance magnetic spectrometer consisting of a large-aperture quadrupole singlet followed by a dipole magnet. A microchannel plate is located at the entrance to the spectrometer and provides x and y positions and time measurements of ions entering the spectrometer. At the exit of the spectrometer, there is a focal-plane detector system consisting of a multiwire parallel-plate avalanche chamber (MWPPAC), followed downstream by an ionization chamber. The MWPPAC provides x and y positions, and time information of ions once they have passed through the dipole, while the ionization chamber, divided into 10×4 sections, measures ΔE and E of the ions [26,27]. Measurements made with the PRISMA magnetic spectrometer enable a determination of the atomic number Z, the mass number A, the ion charge state Q, and the time of flight of each ion that reaches the focal-plane detector system. In terms of operating parameters, PRISMA has a large solid angle of 80 msr, a momentum acceptance of ±10%, a mass resolution of 1/300 via time-of-flight measurements, and an energy resolution of up to 1/1000. In this experiment, PRISMA was set at an angle of 38° relative to the beam direction with an angular acceptance of ±6° in the reaction plane; the angular range encompassed the grazing angle.

CLARA is a high-granularity γ-ray detector array, consisting of 25 EUROBALL escape-suppressed hyperpure Ge clover detectors, of which 22 were operating during the experiment, mounted in a hemispherical-shaped frame. The CLARA array [24] has a photopeak efficiency of about 3% and a peak-to-total ratio of 0.45 for ^{60}Co 1332-keV γ rays and covers an azimuthal angular range of $\theta = 104°$ to 180° with respect to the entrance to the PRISMA magnetic spectrometer. Following Doppler-shift correction of the energies of γ rays from projectile-like species, the FWHM of γ-ray photopeaks is approximately 1% in energy. A relative photopeak efficiency calibration for the CLARA and GASP arrays was carried out through the use of standard radioactive sources of ^{152}Eu, ^{133}Ba, and ^{56}Co isotopes.

A. Data analysis

In this experiment, each γ ray detected in the CLARA array can be unambiguously associated with a nucleus of known mass number A and atomic number Z. However, it is not in general possible to place the identified γ-ray transitions in a level scheme, since the γ-ray coincidence data from the PRISMA-CLARA experiment lack sufficient statistics. Therefore, γ-γ-γ coincidence data were utilized from the associated GASP experiment, in which the nuclei of interest were populated. The analysis of such data allowed the establishment of coincidence relationships between γ rays assigned to ^{96,97,99}Nb, leading to the level schemes which will be presented later. As noted earlier, it was not possible to construct a level scheme for ^{98}Nb. Figure 1 presents ΔE versus E matrices based on data from the segmented ionization chamber. The upper matrix corresponds to all data, while the lower matrix, through appropriate gates set on A/Q and γ-ray energy, corresponds to ^{96}Zr ions. The Z resolution is adequate to separate neighboring isotopes; however, as may be seen from Fig. 1, the large yield of ^{96}Zr ions does result in some contamination of neighboring isotopes. Figure 2 shows a mass spectrum for the niobium isotopes, based on data from PRISMA. By gating on the mass peak corresponding to a

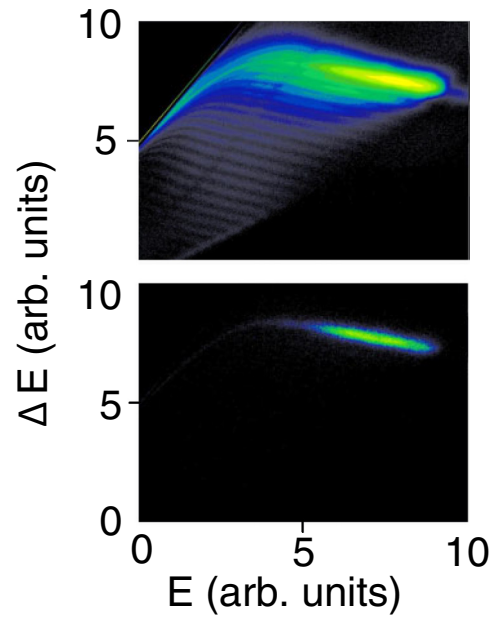

FIG. 1. ΔE versus E matrices based on data from the segmented ionization chamber. The upper matrix corresponds to all data while the lower matrix corresponds to ^{96}Zr ions. See text for details.

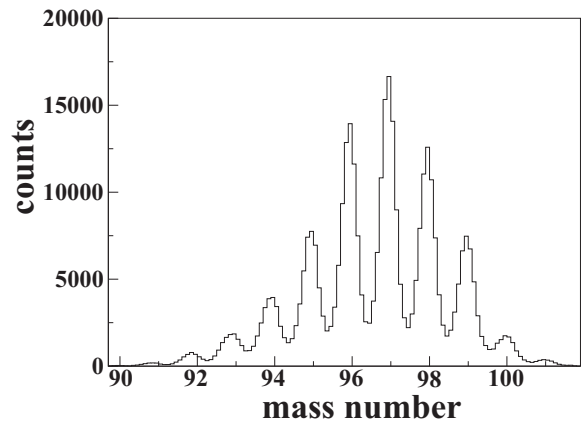

FIG. 2. Mass spectrum of the Nb isotopes detected and identified by the PRISMA spectrometer.

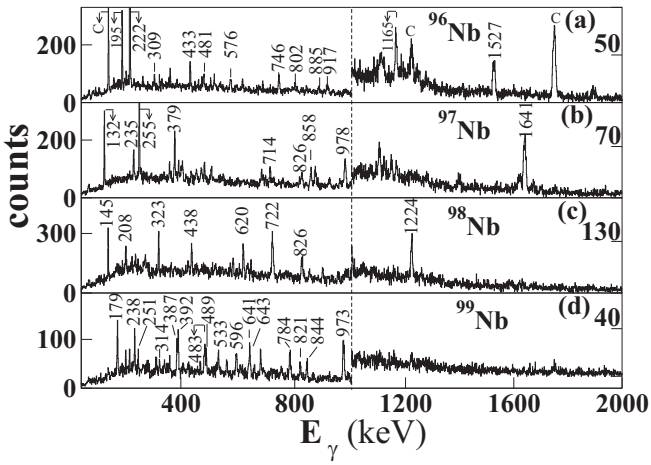

FIG. 3. Doppler-corrected γ-ray spectra measured with the CLARA Ge-detector array in coincidence with the $Z = 41$ Nb isotopes with mass numbers $A = 96$, 97, 98, and 99. "C" indicates contamination peaks from ^{96}Zr. The dashed line indicates a change in the counts scale.

specific isotope, it is possible to obtain from the PRISMA-CLARA coincidence data the associated Doppler-corrected γ-ray spectrum corresponding to the isotope of choice. In particular, by gating on the isotopes of Nb of mass numbers $A = 96$, 97, 98, 99, γ-ray spectra with prominent photopeaks associated with the decay of the yrast states in ^{96,97,98,99}Nb are observed (Fig. 3). Thus, one can unambiguously assign γ-ray transitions to the deexcitation of levels in ^{96,97,98,99}Nb.

Table I lists the transition energies and relative γ-ray photopeak intensities determined from the PRISMA-CLARA experiment. Also shown for each γ-ray transition are the excitation energies of the initial and final states. For ^{98}Nb, none of the γ-ray transitions listed in Table I has previously been reported in the literature. The level schemes for ^{96}Nb and ^{97}Nb from the present work are consistent with those from the work of Fotiades *et al.* [11]. The previously known low-spin level scheme of ^{99}Nb has been extended to high spin $(29/2\ \hbar)$ and two previously unobserved decay sequencies have been identified. In the present work, a few transitions for a given isotope have similar intensities, and this results in potential problems in their relative placement in the level scheme. Proposed spin and parity assignments of the previously unobserved states of ^{99}Nb have been based on a detailed comparison with the known level schemes of neighboring nuclei, as will be described in detail later.

The offline analysis of the GASP data consisted of constructing gated γ-γ matrices. The γ-γ-γ coincidences were sorted into gated γ-γ matrices and double-gated coincidence spectra were constructed using the xtrackn (also known as GASPware [28]) and Radware [29] computer codes. Coincidence γ-γ-γ data from the fusion-fission reaction were used to establish coincidence relationships. As noted above, identification of photopeaks corresponding to the isotopes of Nb studied in the present work was based on the γ-ray transitions observed in the analysis of the PRISMA-CLARA data. Examples of double-gated γ-ray spectra labeled with their associated gates are shown in Fig. 4. Figure 4(a) shows the γ-ray spectrum which corresponds to a double gate placed

TABLE I. Gamma-ray energies and relative intensities for observed transitions in ^{96,97,98,99}Nb. Relative γ-ray intensities are based on the results of the PRISMA-CLARA experiment and are normalized to the strongest transition in each isotope. Also shown, for each γ-ray transition, are the excitation energies of the initial and final states. The uncertainty in transition energies is estimated to be 1 keV. The symbol "*" indicates that the transition was not observed in the PRISMA-CLARA experiment but was observed in the GASP experiment.

^{96}Nb			^{97}Nb			^{98}Nb		^{99}Nb		
E_γ(keV)	I_γ	$E_i \rightarrow E_f$ (keV)	E_γ(keV)	I_γ	$E_i \rightarrow E_f$ (keV)	E_γ(keV)	I_γ	E_γ(keV)	I_γ	$E_i \rightarrow E_f$ (keV)
195.0	38(1)	1944 → 1749	131.6	64(1)	1773 → 1641	145.2	40(1)	86.7	*	631 → 544
221.5	100	222 → 0	234.7	15(1)	4099 → 3864	208.3	17(2)	178.5	49(2)	544 → 365
308.6	7(1)	3262 → 2953	237.9	*	2751 → 2513	323.4	35(1)	238.4	27(2)	869 → 631
433.4	23(1)	2377 → 1944	254.6	48(1)	3006 → 2751	438.2	31(1)	251.1	14(2)	1120 → 869
480.7	11(1)	4545 → 4064	379.4	26(1)	4099 → 3720	620.3	54(1)	281.9	7(1)	1402 → 1120
576.2	8(2)	2953 → 2377	392.8	5(2)	4257 → 3864	722.4	100	314.4	11(1)	1716 → 1402
745.6	21(2)	2133 → 1387	484.1	13(1)	5409 → 4925	826.3	60(1)	325.2	4(1)	869 → 544
801.6	13(2)	4064 → 3262	561.2	*	4661 → 4099	1224.2	95(1)	326.7	3(1)	2043 → 1716
885.1	9(2)	3262 → 2377	714.4	19(2)	3720 → 3006			387.4	33(2)	387 → 0
917.1	13(2)	3050 → 2133	825.7	15(2)	4925 → 4099			391.9	39(2)	2149 → 1757
1164.8	39(2)	1387 → 222	858.4	22(2)	3864 → 3006			483.4	31(2)	869 → 387
1009.0	*	2953 → 1944	872.2	20(2)	2513 → 1641			489.1	17(2)	1120 → 631
1527.1	52(2)	1749 → 222	959.3	8(1)	3472 → 2513			533.1	19(1)	1402 → 869
			969.4	*	3720 → 2751			596.0	20(1)	1716 → 1120
			978.1	60(3)	2751 → 1773			640.5	12(1)	2043 → 1402
			1072.4	*	4544 → 3472			643.0	17(2)	2359 → 1716
			1640.5	100	1641 → 0			784.2	56(2)	1757 → 973
								820.8	22(1)	3814 → 2993
								844.3	28(2)	2993 → 2149
								972.9	100	973 → 0

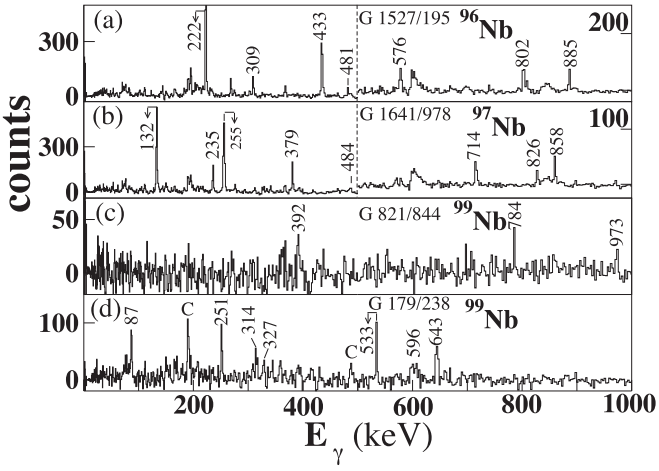

FIG. 4. Double-gated γ-ray spectra of the ^{96,97,99}Nb isotopes. "c" indicates contamination from complementary fragments. Spectrum (a) corresponds to a double gate set on the 195- and 1527-keV transitions of ^{96}Nb, spectrum (b) corresponds to a double gate set on the 978- and 1641-keV transitions of ^{97}Nb, spectrum (c) corresponds to a double gate set on the 844- and 821-keV transitions of ^{99}Nb, while spectrum (d) corresponds to gates set on the 238- and 179-keV transitions of ^{99}Nb. The dashed line indicates a change in the counts scale.

on the 195- and 1527-keV γ-ray photopeaks; labeled peaks correspond to transitions in ^{96}Nb. Unlabeled peaks are from the complementary fission partners detected in coincidence. Similarly, Figs. 4(b), 4(c), and 4(d) correspond to double gates on transitions of energy 978 and 1641 keV in ^{97}Nb, 821 and 844 keV in ^{99}Nb, and 179 and 238 keV in ^{99}Nb, respectively.

The level schemes of ^{96,97,99}Nb were constructed from such coincidence spectra. In the GASP data, prompt γ rays emitted by complementary fission fragments are detected in coincidence with transitions in the Nb isotopes and their photopeaks are thus observed in the coincidence spectra, as noted above. The statistics in both experiments were insufficient to carry out a γ-ray angular correlation analysis; consequently, it is not possible to make robust spin assignments to populated states.

B. Level scheme of ^{96}Nb

The level structure of ^{96}Nb has been investigated in a number of published works. States of low spin have been studied in the ^{96}Zr$(p, n\gamma)$ reaction [30]; in this and in earlier $(p, n\gamma)$ studies (see Ref. [13] and references therein), tentative J^π assignments were made for states of excitation energy up to 1.6 MeV. One- and two-nucleon transfer reactions [12,31–33] have been used to identify states of excitation energy up to 2.96 MeV. In the ^{96}Zr(^{3}He, t) charge-exchange reaction [31], six low-lying states which belong to the $(\pi g_{9/2})(\nu d_{5/2})^{-1}$ configuration were identified. The highest spin member of the multiplet, assigned (7^+), was associated with the 233-keV state. As expected from simple shell-model considerations, the members of the multiplet were also populated in the ^{97}Mo$(t, \alpha)^{96}$Nb proton pickup reaction [12]; in addition, the two states which correspond to the coupling $(\pi p_{1/2})(\nu d_{5/2})^{-1}$ were identified. The low-spin level structure based on the above references has been evaluated by Abriola and Sonzogni [13]. High-spin yrast states of ^{96}Nb were subsequently investigated by Fotiades *et al.* [11] through the study of γ rays following two different fusion-fission reactions; spin assignments for the observed states were not possible experimentally. Fotiades *et al.* associated the lowest-lying state at 222 keV with the previously observed 233-keV state [12,31,32] with a J^π assignment of (7^+). However, it is noted that the excitation energy of 221.7(1.0) keV measured by Fotiades *et al.* [11] is not in agreement with that adopted in the Nuclear Data Sheets evaluation [13], namely 233(5) keV. The present work is in agreement with the excitation energy quoted by Fotiades *et al.* [11], namely 221.5(1.0) keV. It would therefore appear that the tentative spin assignment of (7^+) made by Fotiades *et al.* [11] for the 222-keV state is incorrect. While all ^{96}Nb transitions observed in the present work were previously reported by Fotiades *et al.* [11], the work described here does significantly lead to an unambiguous association of the decay sequence first observed by Fotiades *et al.* [11] with the ^{96}Nb nucleus; this is particularly important, since none of the γ-ray transitions observed by Fotiades *et al.* had previously been observed. Figure 5 presents a comparison of the level scheme of the present work with those of Fotiades *et al.* [11], the (^{3}He, t) work of Comfort *et al.* [31], and the $(p, n\gamma)$ work of Cochavi and Fossan [34].

C. Level scheme of ^{97}Nb

The Nuclear Data Sheets evaluation of $A = 97$ isobars [16] predates the first high-spin study of ^{97}Nb by Fotiades *et al.* [11] and, for ^{97}Nb, was partially based on a number of β-decay studies, the first of which was the work of Siivola *et al.* [14]. Subsequent β-decay studies were used to inform the evaluated level scheme and decay γ rays; see Ref. [16]. Proton-particle and proton-hole states were identified in the ^{96}Zr(^{3}He, d)^{97}Nb [35] single proton-stripping reaction and in the ^{98}Mo(d, ^{3}He)^{97}Nb [36] and ^{98}Mo(t, α)^{97}Nb [37] single-proton pickup reactions, respectively. The subsequent high-spin fusion-fission studies of Fotiades *et al.* [11] resulted in the population of states up to an excitation energy of 6626 keV and J^π values up to $(29/2^+)$; none of the observed excited states had previously been reported in the literature. For ^{97}Nb, all transitions observed in the present work, other than that at an energy of 561 keV, have previously been observed [11]. Figure 6 presents a comparison of the level scheme of the present work with those of Fotiades *et al.* [11] and Flynn *et al.* [37]. For the level scheme based on the present work J^π values are those from the earlier published works discussed above. As in the case of ^{96}Nb, the present work importantly provides an unambiguous association of the observed γ-ray transitions, first observed by Fotiades *et al.* [11], with the ^{97}Nb nucleus.

D. Level scheme of ^{99}Nb

For the third isotope of niobium studied here, ^{99}Nb, the evaluation published in 2017 [17] involved states of low angular momentum populated in β decay (the most recent

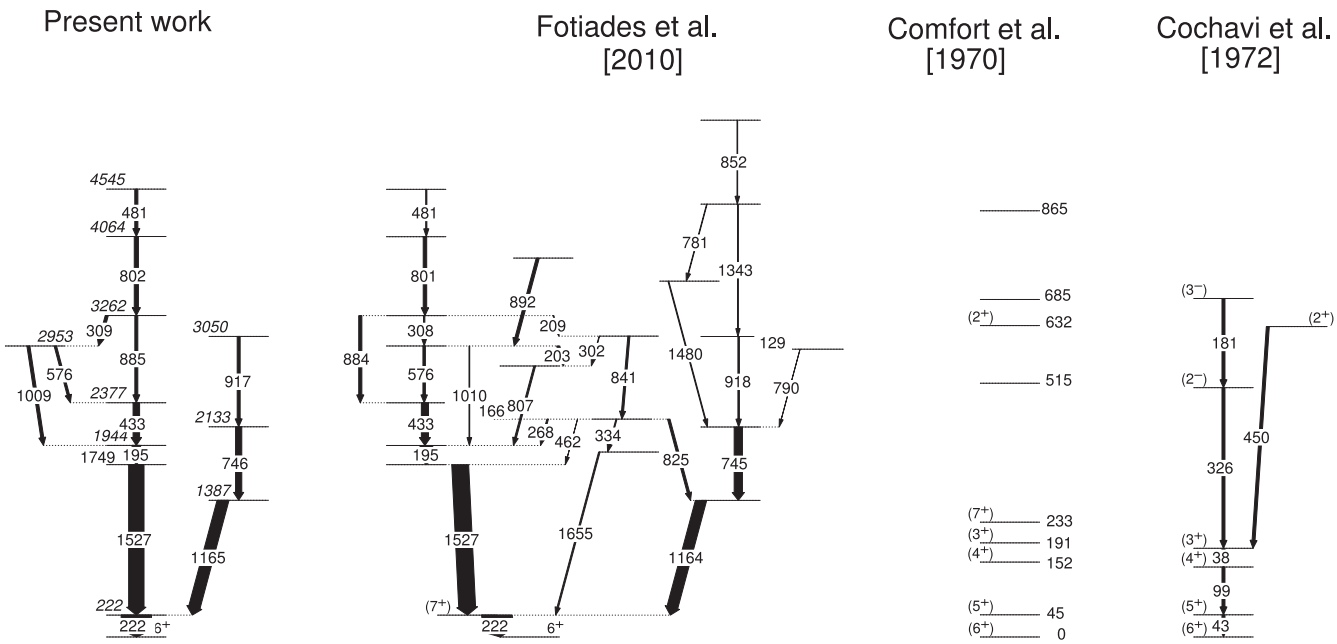

FIG. 5. Level scheme of ^{96}Nb from the present work and from Fotiades *et al.* [11], Comfort *et al.* [31], and Cochavi and Fossan [34]. The present work and that of Fotiades *et al.* [11] result in the population of yrast and near-yrast states. The levels which are populated in the (^{3}He, t) charge-exchange transfer reaction [31] depend on the microscopic structure of the initial and final nuclear states, while the (p, $n\gamma$) study [34] proceeds via compound-nucleus formation and populates low-spin states. For the present work, only the ground-state spin and parity are shown. See the text for details. Energies are in units of keV. Note the change in excitation-energy scale between the two level schemes on the left of the figure with the two on the right of the figure.

study being Ref. [38]) and in the direct proton pickup reactions, ^{100}Mo(d, ^{3}He) [36] and ^{100}Mo(t, α) [37]. The ground state with $J^\pi = 9/2^+$ has the highest spin value of states previously studied. Most of the γ-ray transitions observed in the present work have not previously been reported in the literature; the exceptions to this are the γ-ray transitions [17,38] of energy 87 keV ($5/2^- \rightarrow 3/2^-$), 179 keV ($3/2^- \rightarrow 1/2^-$), and 387 keV ($7/2^+$) $\rightarrow 9/2^+$). Figure 7 presents a comparison of the level scheme of the present work with those of Lhersonneau *et al.* [38] and Flynn *et al.* [37]. The 2017 evaluation [17] has a $J^\pi = (7/2^+)$ assignment for the 387.4-keV level rather than the absence of parentheses in the work of Lhersonneau *et al.* [38]. For the level scheme of the present work, proposed tentative J^π values, presented in parentheses in Fig. 7, will be justified in the following section.

III. DISCUSSION

A. Level systematics and tentative J^π assignments

The fusion-fission and binary grazing reactions employed here preferentially populate yrast and near-yrast states. Figure 8 shows a comparison of the positive-parity yrast level structures of ^{95,97,99}Nb with those of their Zr and Mo isotones. The yrast level structure of ^{95}Nb was taken from the work of Bucurescu *et al.* [39]. The level schemes for the Zr and Mo isotopes are based on Refs. [40–46]; the J^π values for the yrast states of the Mo and Zr isotopes presented in the figure are consistent with the Nuclear Data Sheets evaluations [13,47–49]. For ^{95}Nb, the experimental J^π values for the yrast sequence, established to spin (33/2), and adopted in the evaluation of Basu *et al.* [50], were based on γ-ray angular distribution and angular correlation measurements. It was previously observed [39] that the first two yrast transitions of the assumed $g_{9/2}$ structure in ^{95}Nb [$(13/2^+) \rightarrow 9/2^+$ and $(17/2^+) \rightarrow (13/2^+)$] follow smoothly the trend given by the closest $N = 54$ neighbors (^{96}Mo and ^{97}Tc). As may be seen from Fig. 8, in relation to a comparison with the positive-parity yrast states of ^{96}Mo, this evolution persists for higher spin states, although the correlation is less good. For ^{97}Nb, the yrast level scheme of Fig. 8 is based on the work of Fotiades *et al.* [11]. Tentative spin and parity values, difficult to establish experimentally because of the lack of γ-ray directional correlational information for fission products, were based on a comparison [11] with the ^{96}Zr level scheme. In particular, a one-to-one correspondence was observed between the ^{97}Nb and ^{96}Zr positive-parity yrast excitations. Specifically, the $(29/2^+) \rightarrow (25/2^+) \rightarrow (21/2^+) \rightarrow (17/2^+) \rightarrow (13/2^+) \rightarrow 9/2^+$ sequence of ^{97}Nb is similar to the $(10^+) \rightarrow 8^+ \rightarrow 6^+ \rightarrow 4^+ \rightarrow 2^+ \rightarrow 0^+$ sequence of ^{96}Zr. It is noted that the subshell closure at $N = 56$ results in an increased excitation energy of the first 2^+ state of ^{96}Zr. In Fig. 8, the level scheme presented for ^{99}Nb is based on the present work. In this case, a direct comparison can again be made between the yrast sequences in ^{99}Nb and ^{98}Zr, which leads to tentative J^π assignments in ^{99}Nb of $(13/2^+)$, $(17/2^+)$, $(21/2^+)$, $(25/2^+)$, and $(29/2^+)$ to the states of excitation energy 973, 1757, 2149, 2993, and 3814 keV, respectively. As for ^{95}Nb and ^{97}Nb, the comparison of the excited states with those of the core becomes less good with increasing J^π value. The above behavior would suggest the validity of a simple

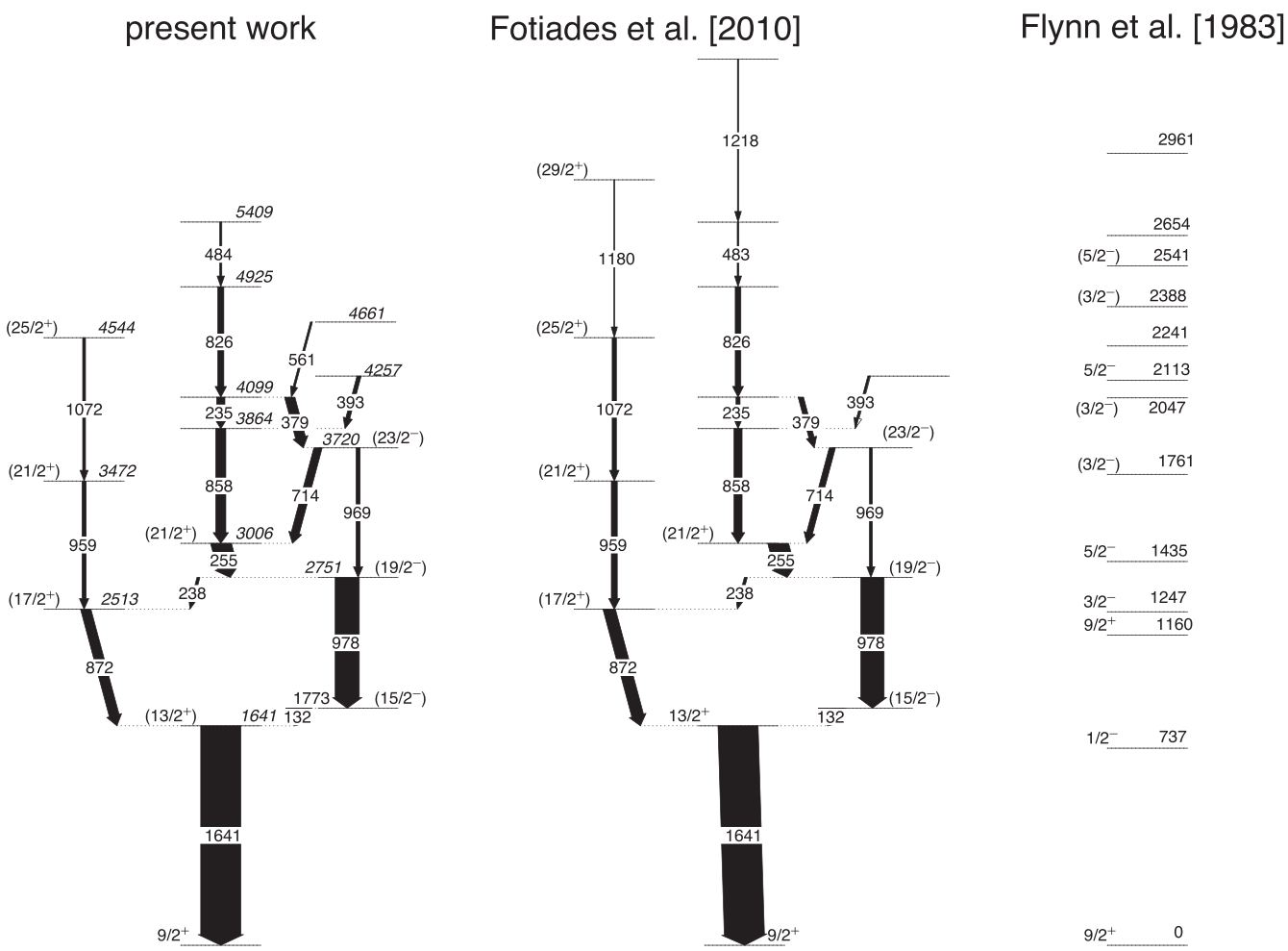

FIG. 6. Level of ^{97}Nb from the present work, from Fotiades *et al.* [11], and from Flynn *et al.* [37]. Yrast and near yrast states are populated in the present work and in that of Fotiades *et al.* [11], while the direct one-proton pickup reaction [37] selectively populates final states with a proton-hole component. Spins and parities of levels populated in the present work are the published values [11]. Note the change in energy scale for the level scheme of Flynn. See text for details. Energies are in units of keV.

model in which the positive-parity yrast states of ^{95}Nb can be described in terms of the coupling of a $1g_{9/2}$ proton hole to the yrast states of the even-even ^{96}Mo core. On the other hand, for ^{97}Nb and ^{99}Nb, the comparison between yrast structures and those of the even-even isotones appears to suggest that there is a better agreement when the coupling of a $1g_{9/2}$ proton with the even-A Zr cores is considered.

It is also instructive to compare the above-proposed positive-parity decay sequence of ^{99}Nb with similar decay sequences in the $N = 58$ isotones, namely ^{97}Y, ^{101}Tc, and ^{103}Rh. Figure 9 presents such a comparison. The positive-parity levels of ^{97}Y are based on the isomer decay study of Lhersonneau *et al.* [51]; the J^π values are those of Nica [16]. For the positive-parity yrast and near yrast decay sequences of ^{101}Tc, the level scheme of Hoellinger *et al.* [52] has been used here; this postdates the evaluation of Blachot [53]. Similarly, for ^{103}Rh, the positive-parity yrast and near yrast decay sequences presented in Fig. 9 are based on the evaluation of De Frenne [54]. It may be seen from Fig. 9 that there are similarities in the positive-parity level structures of the four isotones although again the excitation energies for a given J^π value are not in particularly good agreement. It is also noted that there are close lying doublets in ^{101}Tc and ^{103}Rh which have not been observed in ^{97}Y and in ^{99}Nb. However, for ^{99}Nb, the results of shell-model calculations, to be presented below, do predict a similar doublet structure. The failure to observe such doublets in ^{99}Nb is probably a consequence of the preferential population of yrast states together with low statistics in the present experiment.

Compared to the odd-A isotopes, the larger number of available configurations for the odd-odd Nb isotopes, resulting from the coupling of neutrons and protons, inhibits a meaningful comparison to be made with level schemes in neighboring Mo and Zr isotopes, as was possible above for ^{95,97,99}Nb. In ^{96}Nb, relative to the ^{88}Sr core, there are three protons in the $2p_{1/2}$ and $1g_{9/2}$ shells and five neutrons in the $2d_{5/2}$ and $1g_{7/2}$ shells. The multiplet arising from the $\pi g_{9/2}\ \nu d_{5/2}$ configuration in ^{96}Nb, consisting of six states with J^π values ranging from 2^+ to 7^+, was discussed earlier. A similarity of this multiplet in the ^{92,94,96}Nb isotopes with the corresponding one in the $Z = 43$ isotones ^{94,96,98}Tc has been noted earlier [55]. A comparison of the yrast structures for the high spin

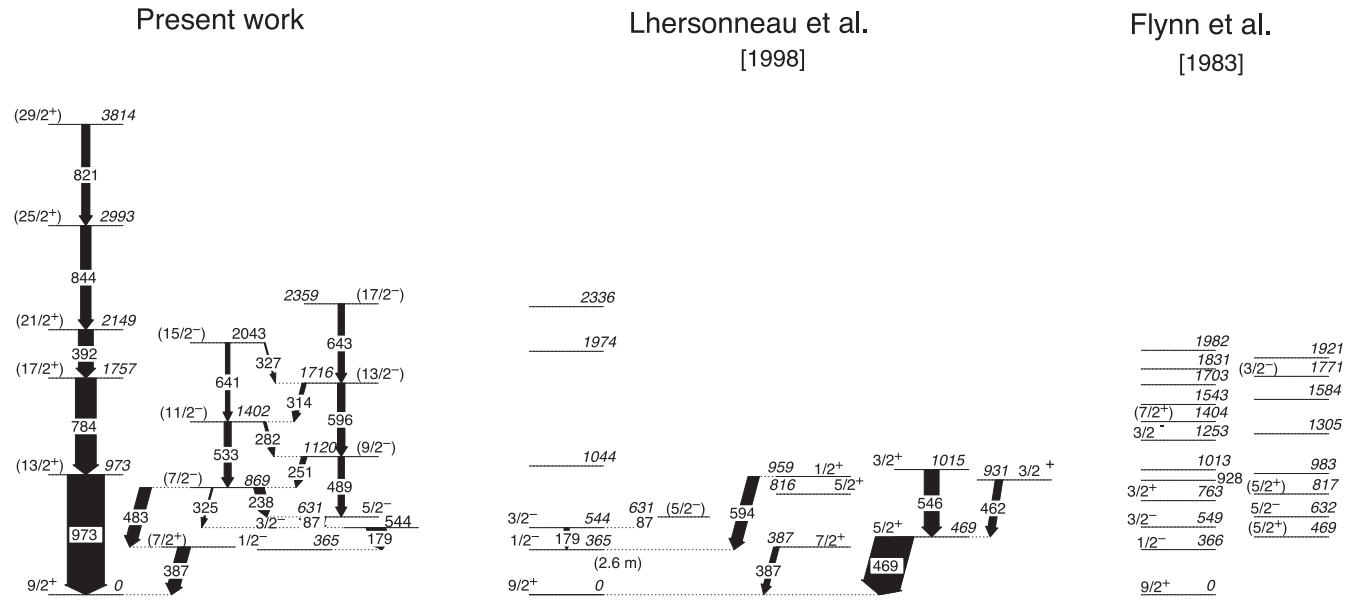

FIG. 7. Level scheme of ^{99}Nb from the present work, from Lhersonneau *et al.* [38], and Flynn *et al.* [37]. Levels populated in the present work are mainly yrast and near yrast. The β decay of ^{99}Zr ($J^\pi = 1/2^+$) [38] populates final states with spin values which differ by only a few units of angular momentum from that of the parent nucleus, while the direct one-proton pickup reaction ^{100}Mo(t, α) reaction [37] selectively populates final states with a proton-hole component. Spins and parities for the level scheme based on the present work are the accepted values from the evaluation of Browne and Tuli [17]; additional tentative J^π values have been made for the members of the rotational sequence based on the $5/2^-$ state at 631 keV and for the members of the decay sequence based on the $9/2^+$ ground state. See text for details. Energies are in units of keV.

states of ^{92}Nb and of ^{94}Nb with those of the ^{94,96}Tc isotones was previously discussed by Mărginean *et al.* [56]. For states with $J^\pi \leqslant (13^+)$, there is a marked similarity between the positive-parity yrast level schemes of ^{92}Nb [57,58] and ^{94}Tc [47,59]; however, the ^{94}Tc level scheme is compressed in energy relative to that of ^{92}Nb. Similarly, the odd-spin positive-parity yrast sequences from $J^\pi = 7^+$ to (17) in ^{94}Nb [56] and in ^{96}Tc [60] are similar, although the differences in excitation energy become increasingly larger with increasing spin. Extending such a comparison to the yrast states of the $N = 55$ isotones, ^{96}Nb and ^{98}Tc is unfortunately not possible at the present time as a consequence of the absence of spin assignments for the yrast states of ^{96}Nb [11] with $J > 7$ and the more complex level structure for ^{98}Tc [61,62] compared with those of the lighter Tc isotopes with $N = 51$ [47,59] and $N = 53$ [13,60].

As discussed above, one of the new features of the ^{99}Nb level scheme is a strong decay sequence based on the $9/2^+$ ground state and with tentative J^π values of $(13/2^+)$, $(17/2^+)$, $(21/2^+)$, $(25/2^+)$, and $(29/2^+)$; see Fig. 7. Such a decay sequence has not been observed in the neighboring higher-mass-number ^{101}Nb [9,63,64] and ^{103}Nb [64,65] isotopes; for these two nuclei, the ground state forms the bandhead

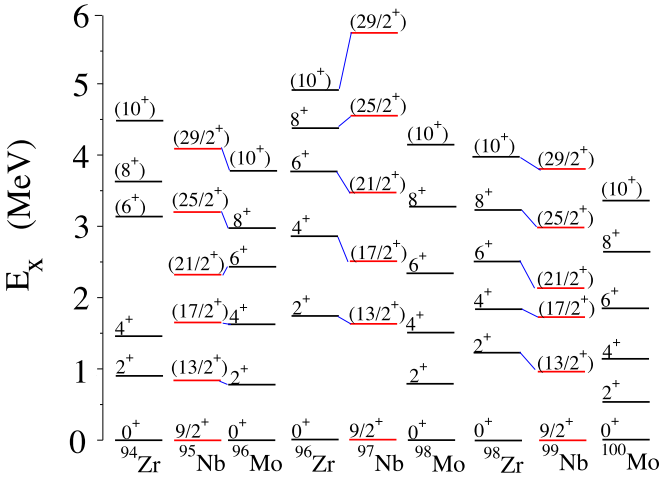

FIG. 8. The positive-parity yrast energy levels of the Nb isotopes with $A = 95$, 97, and 99 compared with the those of the even-even Zr and Mo cores. See text for details.

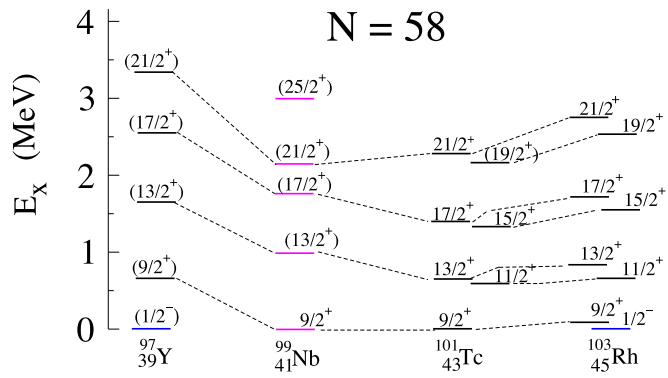

FIG. 9. The positive-parity yrast and near-yrast decay sequences of the $N = 58$ isotones ^{97}Y, ^{99}Nb, ^{101}Tc, and ^{103}Rh. See text for details.

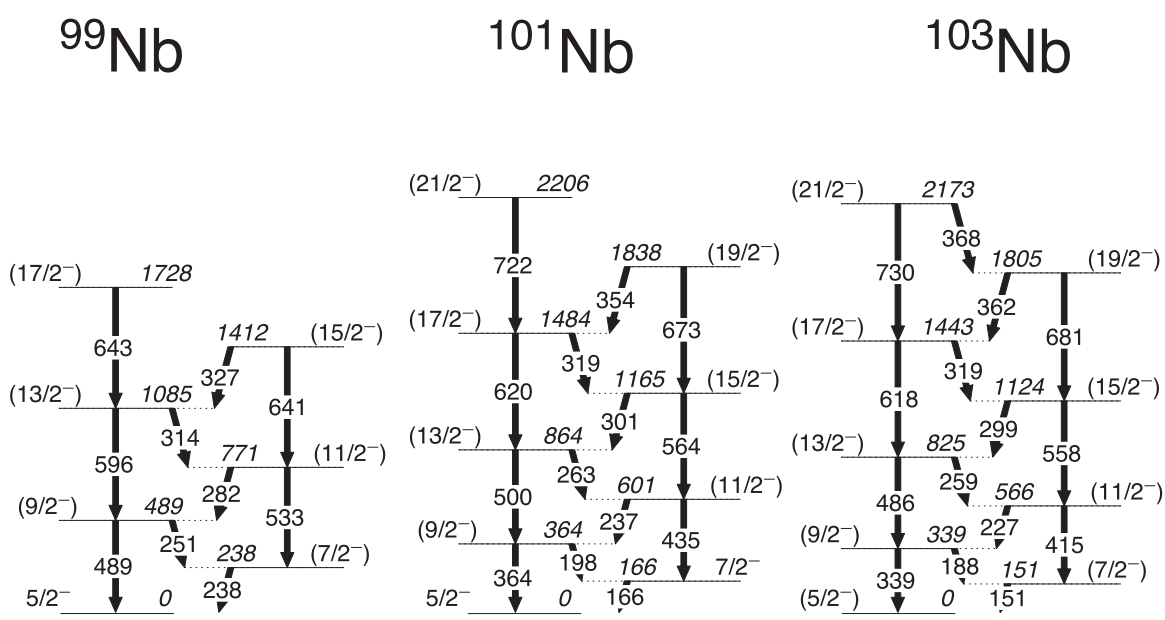

FIG. 10. The rotational sequences of ^{99}Nb, ^{101}Nb, and ^{103}Nb based on $5/2^-$ states. See text for details.

of a $5/2^+[422]$ rotational sequence, which is based on the spherical $1g_{9/2}$ proton orbital. The quadrupole deformation parameters for the $5/2^+[422]$ bands of ^{101}Nb and ^{103}Nb, based on a comparison of the level energies with the results of triaxial particle-plus-rotor model calculations, are $\epsilon_2 = 0.25$ and 0.37, respectively with corresponding γ values of -5° and -15° [9]. Thus, the ground-state quadrupole deformation observed in ^{101}Nb and ^{103}Nb is absent in ^{99}Nb. Indeed, based on its measured quadrupole moment [66] ($Q_s = -0.42$ eb), the ground state of ^{99}Nb ($N = 58$) is expected to be weakly oblate. The second notable feature consists of a previously unobserved bandlike structure based on the known $5/2^-$ state of ^{99}Nb at 631 keV. Similar band structures have been observed in ^{101}Nb [9,63,64] and in ^{103}Nb [64,65], with assigned Nilsson quantum numbers $5/2^-[303]$. The $5/2^-[303]$ decay sequence has also been observed in the adjacent odd-A isotones of ^{101}Nb (^{99}Y [17] and ^{103}Tc [54]) and of ^{103}Nb (^{101}Y [53] and ^{105}Tc [67]). However, the decay sequence has not, to date, been observed in the $N = 58$ isotones, ^{97}Y and ^{101}Tc. On the basis of a comparison with the band structures of ^{101}Nb and ^{103}Nb, see Fig. 10, tentative J^π values of $(7/2^-)$, $(9/2^-)$, $(11/2^-)$, $(13/2^-)$, $(15/2^-)$, and $(17/2^-)$ are assigned to the states of ^{99}Nb at excitation energies of 869, 1120, 1402, 1716, 2043, and 2359 keV, respectively. Figure 7 includes these tentative J^π values for the members of this previously unobserved band, presumably also with Nilsson quantum numbers $5/2^-[303]$. There is thus evidence for shape coexistence at low spin in ^{99}Nb and this will be discussed further below.

B. Comparison with shell-model calculations

Proton occupancies near the Fermi surface of the even-Z isotopes adjacent to niobium have been investigated using single proton pickup and stripping reactions, to which reference has been given above. In a simple shell-model picture of the Nb ($Z = 41$) isotopes, the ground-state proton configuration is $\pi(1f_{5/2})^6(2p_{3/2})^4(2p_{1/2})^2(1g_{9/2})^1$. That the proton shell closure at $Z = 40$ is not robust is illustrated by the presence of $\ell = 1$ strength in the ^{96}Zr(^{3}He, d)^{97}Nb data [35]; the $2p_{3/2}$ and $2p_{1/2}$ proton orbitals should, in a simple shell-model picture, be full in the ground states of the Zr ($Z = 40$) isotopes. The reduction of $1p$ strength is compensated by an increase in $1g_{9/2}$ strength, as is apparent from the measured spectroscopic factors for $\ell = 4$ proton pickup from the (even-A) isotopes ^{90}Zr, ^{92}Zr, ^{94}Z, and ^{96}Zr [68]. The spectroscopic factor for $1g$ proton pickup, C^2S, is approximately 1 [68]; in a simple shell-model description of the ground states of the Zr isotopes, the proton $1g_{9/2}$ occupancy is zero. Such departures from the expectations of the simple shell model at shell and subshell closures are not unusual. In relation to the occupancy of neutron shell-model orbitals, in ^{99}Nb, for example, the neutron configuration in a simple shell-model picture is $(1g_{9/2})^{10}(2d_{5/2})^6(1g_{7/2})^2(2d_{3/2})^0(3s_{1/2})^0(1h_{11/2})^0$.

To understand the microscopic structure of the Nb isotopes studied here, spherical shell-model calculations have been performed using the NuShellx code [69]. The gl, glekpn, and jj45pn model spaces and the residual interactions named gl, glekpn, and jj45pna [70–72] in the code were used. The gl model space includes two valence proton orbitals, $2p_{1/2}$ and $1g_{9/2}$, and two valence neutron orbitals, $2d_{5/2}$ and $3s_{1/2}$. The glekpn model space includes five valence proton orbitals, $1f_{7/2}$, $1f_{5/2}$, $2p_{3/2}$, $2p_{1/2}$, and $1g_{9/2}$, and five valence neutron orbitals, $1g_{9/2}$, $1g_{7/2}$, $2d_{5/2}$, $2d_{3/2}$, and $3s_{1/2}$, while the jj45pn model space includes four valence proton orbitals, $1f_{5/2}$, $2p_{3/2}$, $2p_{1/2}$, and $1g_{9/2}$, and five valence neutron orbitals, $1g_{7/2}$, $2d_{5/2}$, $2d_{3/2}$, $3s_{1/2}$, and $1h_{11/2}$.

The residual interaction contains a combination of calculated and empirical two-body matrix elements as described in Ref. [73]. In the present calculations, $^{88}_{38}$Sr$_{50}$ was assumed to be an inert core, as was the case in the published shell-

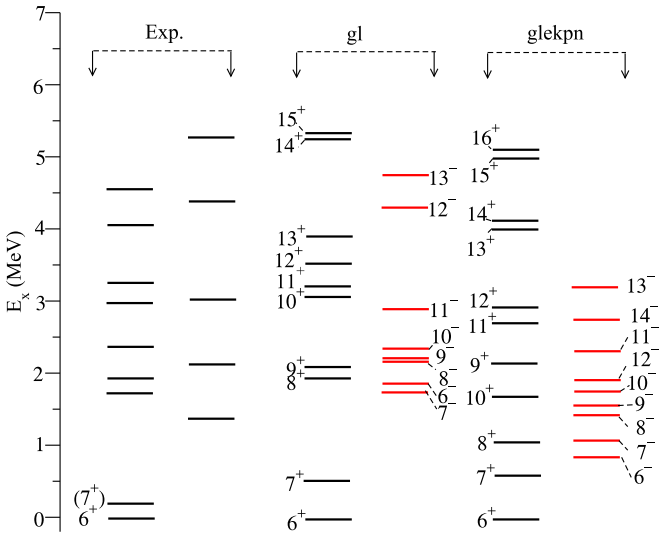

FIG. 11. Comparison of the experimental energy levels of ^{96}Nb (left) with theoretical predictions, in the middle with gl, and on the right with glekpn model spaces using the NuShellx code [69]. Details may be found in the text.

model description of ^{94,95}Nb [39,56]. The construction of gl and glekpn interactions based on the proton-proton, neutron-neutron, and proton-neutron effective interactions by a least-squares fitting procedure is discussed in Refs. [70,71,74]. The jj45pna interaction is composed of four parts, namely proton-proton, neutron-neutron, and proton-neutron interactions, as well as a Coulomb repulsive term. The proton-proton, neutron-neutron, and proton-neutron interactions were derived from the charge-dependent Bonn potential (CD-Bonn) based on the predictions of the Bonn full model [75–77] used in the description of the nucleon-nucleon interaction.

Truncations applied to the glekpn model space involved the full occupation of the proton $1f_{7/2}$, $1f_{5/2}$, and $2p_{3/2}$ orbitals and full occupation of the $1g_{9/2}$ neutron orbital, and the jj45pn model space involved the full occupation of the proton $1f_{5/2}$ and $2p_{3/2}$ orbitals. As the calculations lead to too large dimensions to be performed in the full jj45pn space, a truncation of the neutron valence space was also made by keeping the $1h_{11/2}$ orbit empty. We presume that this constitutes an appropriate truncation for the description of the lowest excited states of ^{97,99}Nb, since the $\nu h_{11/2}$ orbit is expected to be involved only for states of higher spins at high excitation energies. A similar truncation was used in a shell-model calculation of the lowest excited states of ^{100}Ru [78]. Here the calculations have been made up to $I = 16$.

Figures 11–13 present a comparison of the experimental energy levels (shown on the left) with shell-model predictions (in the middle and right) for ^{96}Nb, ^{97}Nb, and ^{99}Nb, respectively. Tables II, III, and IV show the nucleon occupations of the orbitals included in the calculations.

In Fig. 11, the experimental levels, yrast and near yrast, are those of Fotiades *et al.* [11]. The corresponding shell-model calculations, which show the positive- and negative-parity yrast states, correctly reproduce the spins and parities of the ground and 233-keV states. As expected (see Table II), the wave functions of the two states correspond, to a good approximation, to the configuration $(\pi g_{9/2})(\nu d_{5/2})^{-1}$. It is noted that the present shell-model calculations fail to reproduce the observed doublet, discussed above, at 222/233 keV. The absence of spin-parity assignments for the other states presented in Fig. 11 makes a comparison of experiment with shell model not possible. A comparison of the experimental level scheme with the results of the shell-model calculations

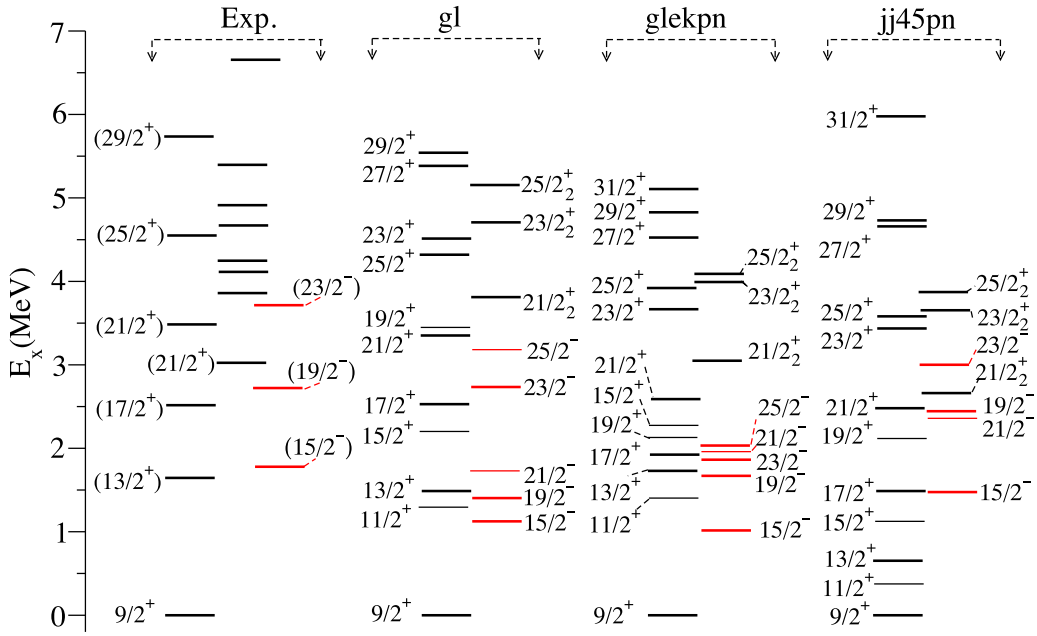

FIG. 12. Comparison of the experimental energy levels of ^{97}Nb (left) with theoretical predictions, in the middle with gl and glekp, and on the right with jj45 model space using the NuShellx code [69]. Details may be found in the text.

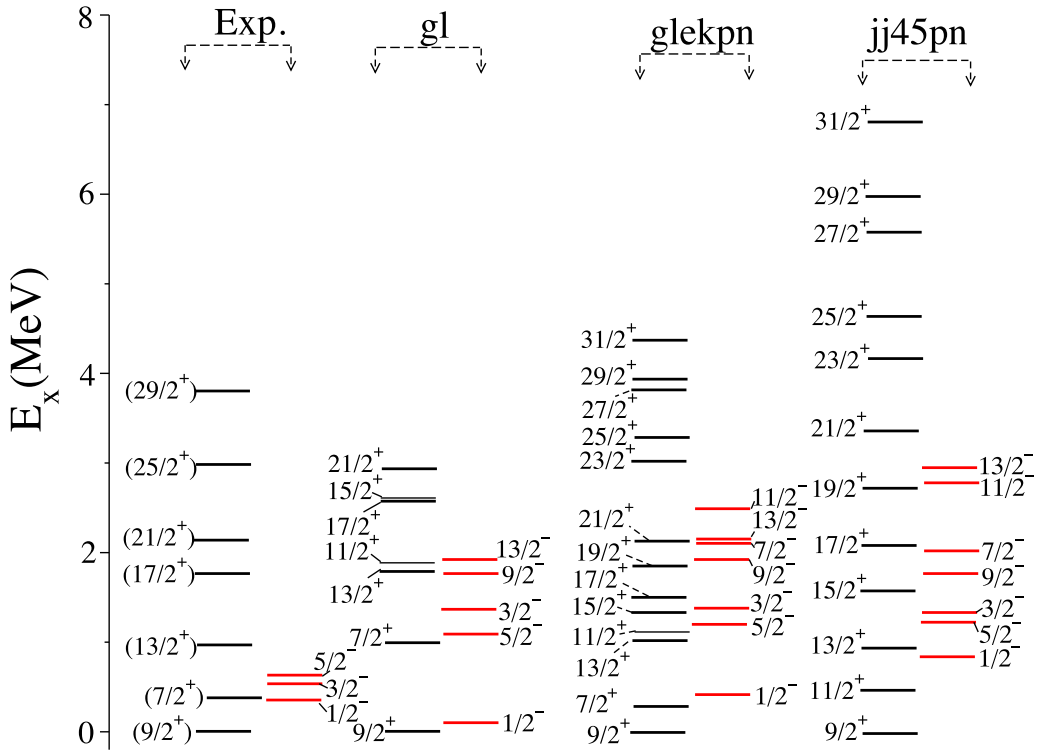

FIG. 13. Comparison of the experimental energy levels of ^{99}Nb (left) with theoretical predictions, in the middle with gl and glekpn, and on the right with jj45 model space using the NuShellx code [69]. Details may be found in the text.

corresponding to the gl model space suggests that the states at excitation energies of 1745 and 1944 keV are associated with the shell-model yrast 8^+ and 9^+ states; however, this highly speculative conclusion is not supported by the level scheme corresponding to the glekpn model space. It is noted that for the positive-parity states with $J^\pi \geqslant 10^+$ there is no proton occupation of the $2p_{1/2}$ orbital for the gl model space and this leads to different $1g_{9/2}$ proton occupations in the gl and glekpn

TABLE II. Occupation numbers of the spherical orbitals used in the present shell-model calculations for ^{96}Nb.

	gl					glekpn										
	E_x	Protons		Neutrons		E_x	Protons					Neutrons				
State	keV	$2p_{1/2}$	$1g_{9/2}$	$3s_{1/2}$	$2d_{5/2}$	keV	$1f_{7/2}$	$1f_{5/2}$	$2p_{3/2}$	$2p_{1/2}$	$1g_{9/2}$	$1g_{9/2}$	$1g_{7/2}$	$2d_{5/2}$	$2d_{3/2}$	$3s_{1/2}$
6^+	0	1.70	1.30	0.24	4.76	000	8.00	6.00	4.00	1.89	1.11	10.00	0.03	4.64	0.12	0.21
7^+	514	1.50	1.50	0.44	4.56	608	8.00	6.00	4.00	1.83	1.17	10.00	0.04	4.54	0.13	0.30
8^+	1953	0.48	2.52	1.45	3.55	1072	8.00	6.00	4.00	1.48	1.52	10.00	1.02	3.28	0.21	0.48
9^+	2096	0.24	2.76	1.73	3.27	2168	8.00	6.00	4.00	0.60	2.40	10.00	1.00	2.99	0.20	0.81
10^+	3078	0.00	3.00	1.50	3.50	1709	8.00	6.00	4.00	1.74	1.26	10.00	1.01	3.57	0.12	0.29
11^+	3213	0.00	3.00	1.76	3.24	2724	8.00	6.00	4.00	1.24	1.76	10.00	1.02	3.13	0.17	0.68
12^+	3531	0.00	3.00	1.61	3.39	2912	8.00	6.00	4.00	1.63	1.37	10.00	1.01	3.49	0.13	0.37
13^+	3903	0.00	3.00	1.63	3.37	4032	8.00	6.00	4.00	0.34	2.66	10.00	1.67	2.18	0.17	0.97
14^+	5247	0.00	3.00	1.94	3.06	4116	8.00	6.00	4.00	0.08	2.92	10.00	1.88	1.81	0.26	1.05
15^+	5260	0.00	3.00	2.00	3.00	4982	8.00	6.00	4.00	0.35	2.65	10.00	1.83	2.18	0.17	0.82
6^-	1872	1.00	2.00	0.60	4.40	841	8.00	6.00	4.00	1.00	2.00	10.00	1.01	3.11	0.31	0.57
7^-	1750	1.00	2.00	0.39	4.61	1085	8.00	6.00	4.00	1.00	2.00	10.00	0.09	4.34	0.16	0.42
8^-	2196	1.00	2.00	0.80	4.20	1437	8.00	6.00	4.00	1.00	2.00	10.00	0.08	3.79	0.20	0.93
9^-	2187	1.00	2.00	0.29	4.71	1563	8.00	6.00	4.00	1.00	2.00	10.00	0.06	4.47	0.14	0.33
10^-	2356	1.00	2.00	0.70	4.30	1754	8.00	6.00	4.00	1.00	2.00	10.00	0.08	4.03	0.15	0.74
11^-	2909	1.00	2.00	0.63	4.37	2320	8.00	6.00	4.00	1.00	2.00	10.00	0.09	4.06	0.17	0.68
12^-	4309	1.00	2.00	1.22	3.78	1933	8.00	6.00	4.00	1.00	2.00	10.00	1.03	3.22	0.21	0.55
13^-	4751	1.00	2.00	1.44	3.56	3199	8.00	6.00	4.00	1.00	2.00	10.00	1.02	3.35	0.11	0.52

TABLE III. Occupation numbers of the spherical orbitals used in the present shell-model calculations for ^{97}Nb. The proton orbits $1f_{7/2}$, $1f_{5/2}$, and $2p_{3/2}$ and neutron orbit $1g_{9/2}$ were kept fully occupied. The neutron orbit $1h_{11/2}$ was kept empty.

	gl					glekpn							jj45pn						
	E_x	Protons		Neutrons		E_x	Protons		Neutrons				E_x	Protons		Neutrons			
State	keV	$2p_{1/2}$	$1g_{9/2}$	$3s_{1/2}$	$2d_{5/2}$	keV	$2p_{1/2}$	$1g_{9/2}$	$1g_{7/2}$	$2d_{5/2}$	$2d_{3/2}$	$3s_{1/2}$	keV	$2p_{1/2}$	$1g_{9/2}$	$1g_{7/2}$	$2d_{5/2}$	$2d_{3/2}$	$3s_{1/2}$
$9/2^+$	0	1.61	1.39	0.46	5.54	0	1.84	1.16	0.06	5.34	0.19	0.41	0	0.06	2.94	1.62	2.91	0.87	0.61
$13/2^+$	1459	0.60	2.40	1.68	4.32	1725	1.31	1.69	0.26	4.34	0.26	1.14	633	0.03	2.97	1.70	2.86	0.87	0.57
$15/2^-$	1165	1.00	2.00	0.86	5.14	1016	1.00	2.00	0.15	4.70	0.25	0.90	1491	1.00	2.00	1.07	3.35	0.74	0.84
$17/2^+$	2538	0.18	2.82	1.94	4.06	1924	1.03	1.97	1.03	3.86	0.20	0.91	1489	0.02	2.98	1.57	2.94	0.92	0.57
$19/2^-$	1395	1.00	2.00	1.34	4.66	1661	1.00	2.00	0.15	4.41	0.24	1.19	2433	1.00	2.00	0.27	3.80	0.85	1.07
$21/2^+$	3386	0.00	3.00	1.79	4.21	2596	1.29	1.71	1.03	4.03	0.18	0.76	2490	0.02	2.98	1.51	3.05	0.95	0.49
$21/2_2^+$	3791	0.00	3.00	1.51	4.49	3067	0.71	2.29	1.04	3.53	0.21	1.22	2693	0.03	2.97	1.21	3.14	1.08	0.56
$23/2^-$	2752	1.00	2.00	1.25	4.75	1886	1.00	2.00	1.00	3.71	0.25	1.04	2992	1.00	2.00	0.32	3.88	0.98	0.82
$23/2^+$	4526	0.00	3.00	1.70	4.30	3673	0.19	2.81	1.06	3.13	0.27	1.54	3459	0.06	2.94	1.21	3.20	0.96	0.63
$23/2_2^+$	4686	0.00	3.00	1.62	4.38	3970	1.51	1.49	1.23	3.47	0.80	0.50	3580	0.05	2.95	1.20	2.83	1.33	0.64
$25/2^+$	4309	0.00	3.00	1.88	4.12	3920	0.14	2.86	1.17	2.97	0.22	1.63	3544	0.01	2.99	1.47	3.07	0.96	0.51
$25/2_2^+$	5162	0.00	3.00	1.90	4.10	4096	0.51	2.49	1.87	3.07	0.22	0.84	3919	0.02	2.98	1.17	2.82	1.11	0.90
$27/2^+$	5374	0.00	3.00	1.95	4.05	4.511	0.04	2.96	1.85	2.14	0.36	1.66	4.687	0.10	2.90	1.24	2.91	1.04	0.80

model spaces. In this particular case, calculations based on the jj45pn model space do not reproduce the experimental energy levels well and are not presented in Fig. 11; for example, the ground-state J^π value is predicted to be 1^+ rather than the experimental 6^+ value.

In Fig. 12, the experimental levels are again those of Fotiades *et al.* [11]. For the proposed positive-parity decay sequence in ^{97}Nb with J^π values in the range from $9/2^+$ to $(29/2^+)$, the correspondence between the experimental and shell-model states is reasonably good, especially for calculations corresponding to the gl model space. Similarly, there is a reasonable correspondence between theory and experiment for the proposed negative-parity states with J^π values of $(15/2^-)$, $(19/2^-)$, and $(23/2^-)$, although, in this case, the agreement with excitation energies is less good. For high-spin positive-parity states, all three extra-core protons occupy the $\pi 1g_{9/2}$ orbital with consequently no occupancy of the $\pi 2p_{1/2}$ orbital.

The proposed positive-parity yrast states of ^{99}Nb, based on the present work, with J^π values in the range from $(9/2^+)$ to $(29/2^+)$, are well described with the glekpn model space; calculations which used the gl and jj45pn model spaces are much less successful over the range of experimental states. See Fig. 13. On the other hand, calculations which employed the jj45pn model space are the most successful in reproducing the first two excited states with spins $13/2^+$ and $17/2^+$. To date, the positive-parity states with J^π values of $11/2^+$, $15/2^+$, $19/2^+$, $23/2^+$, etc., predicted using the glekpn model space, have not been identified experimentally, as was noted above. The shell-model calculation based on the glekpn interaction reproduces the excitation energy of the $1/2^-$ state well, while the jj45pn interaction is the least successful. All three interactions are unable to reproduce the excitation energies of the low-lying negative-parity $J^\pi = 3/2^-$ and $5/2^-$ states and this is especially the case for the jj45pn interaction, see Fig. 13. It will be seen later that model calculations indicate

TABLE IV. Occupation numbers of the spherical orbitals used in the present shell-model calculations for ^{99}Nb. The proton orbits $1f_{7/2}$, $1f_{5/2}$, and $2p_{3/2}$ and neutron orbit $1g_{9/2}$ were kept fully occupied. The neutron orbit $1h_{11/2}$ was kept empty.

	gl					glekpn							jj45pn						
	E_x	Protons		Neutrons		E_x	Protons		Neutrons				E_x	Protons		Neutrons			
State	keV	$2p_{1/2}$	$1g_{9/2}$	$3s_{1/2}$	$2d_{5/2}$	keV	$2p_{1/2}$	$1g_{9/2}$	$1g_{7/2}$	$2d_{5/2}$	$2d_{3/2}$	$3s_{1/2}$	keV	$2p_{1/2}$	$1g_{9/2}$	$1g_{7/2}$	$2d_{5/2}$	$2d_{3/2}$	$3s_{1/2}$
$9/2^+$	0	0.81	2.19	2.00	6.00	0	0.12	2.88	1.88	3.83	0.59	1.70	0	0.01	2.99	2.06	3.48	1.29	1.17
$13/2^+$	1761	0.00	3.00	2.00	6.00	1011	0.04	2.96	2.03	3.71	0.57	1.69	0934	0.01	2.99	2.08	3.48	1.34	1.09
$17/2^+$	2588	0.00	3.00	2.00	6.00	1501	0.07	2.93	1.99	3.81	0.50	1.70	2065	0.01	2.99	1.25	3.94	1.65	1.16
$21/2^+$	2926	0.00	3.00	2.00	6.00	2126	0.16	2.84	2.03	3.85	0.47	1.65	3359	0.02	2.98	1.94	3.73	1.35	0.98
$25/2^+$						3274	0.25	2.75	2.07	3.84	0.33	1.76	4639	0.03	2.97	2.02	3.68	1.31	1.00
$29/2^+$						3919	0.02	2.98	2.11	3.73	0.34	1.82	5979	0.01	2.99	2.06	3.66	1.32	0.96
$1/2^-$	113	1.00	2.00	2.00	6.00	423	1.00	2.00	0.08	5.64	0.37	1.91	867	1.00	2.00	2.02	3.71	1.13	1.15
$3/2^-$	1359	1.00	2.00	2.00	6.00	1386	1.00	2.00	0.09	5.59	0.42	1.90	1318	1.00	2.00	2.04	3.64	1.17	1.15
$5/2^-$	1098	1.00	2.00	2.00	6.00	1255	1.00	2.00	0.09	5.60	0.41	1.90	1275	1.00	2.00	2.03	3.64	1.18	1.15

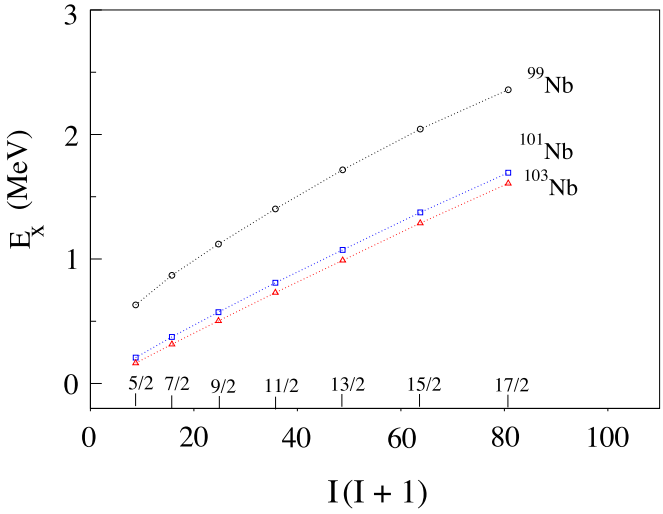

FIG. 14. Energies of the $5/2^-[303]$ band members as a function of $I(I+1)$ for ^{99}Nb, ^{101}Nb, and ^{103}Nb.

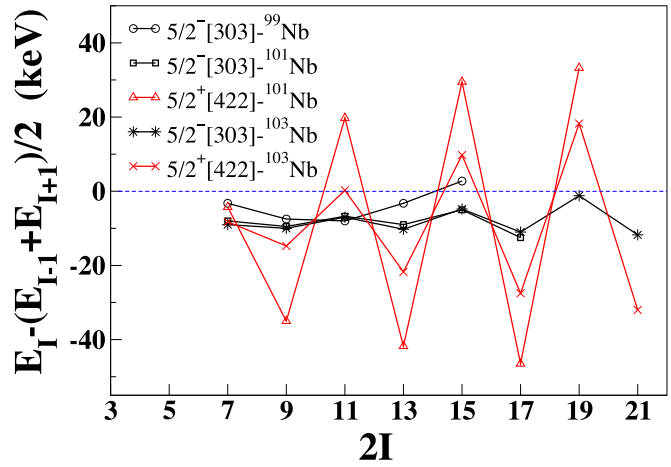

FIG. 15. Signature splitting of the $5/2^+[422]\pi g_{9/2}$ bands of ^{101,103}Nb and the $5/2^-[303]\pi f_{5/2}$ bands of ^{99,101,103}Nb.

that the $5/2^-$ state forms the bandhead of a $5/2^-[303]$ rotational sequence with a quadrupole deformation parameter ϵ_2 of 0.22. At zero deformation, the $5/2^-$ state is based on the spherical $1f_{5/2}$ proton orbital, which is expected to be fully occupied in the Nb isotopes, and this is the assumption in the present shell-model calculations. With increasing quadrupole deformation, the binding energy of the $5/2^-$ bandhead decreases and, for ^{99}Nb, sits at low excitation energy (631 keV). It is therefore not surprising that the shell-model calculations here are unable to reproduce the excitation energy of the state.

C. Signature-splitting, triaxiality, and particle-plus-rotor calculations

With increasing neutron number in the isotopes of niobium, a phase transition to prolate quadrupole deformation is expected near neutron number 60. In $N = 60$ ^{101}Nb, evidence for deformation was first provided by Ohm *et al.* [63]. Three bands populated in the β decay of ^{101}Zr were assigned Nilsson quantum numbers $5/2^+[422]$, $3/2^-[301]$, and $5/2^-[303]$ and a quadrupole deformation parameter of $\beta_2 = 0.40(5)$ was determined for the $5/2^+$ ground state. The moment of inertia of the $5/2^+[422]$ ground band corresponds to about 85% of the rigid body value, which is typical for the $A \sim 100$ region [63]. As noted earlier, the $5/2^+[422]$ band was not observed in ^{99}Nb, but has been observed in ^{101}Nb and in ^{103}Nb. Figure 14 presents the plot of excitation energies as a function of $I(I+1)$ for the $5/2^-[303]$ bands in ^{99}Nb, ^{101}Nb, and ^{103}Nb and shows the expected behavior, with the moments of inertia increasing slowly with increasing angular momentum, presumably as a consequence of the gradual weakening of pairing correlations with increasing rotational frequency. The deduced inertia parameters, $\hbar^2/2\mathcal{J}$, corresponding to the low-spin members of the rotational sequences in ^{99}Nb, ^{101}Nb, and ^{103}Nb, have values of 34, 24, and 22 keV, respectively, corresponding to 43%, 60%, and 66% of the rigid body moment of inertia. As expected, the $5/2^-[303]$ rotational sequence in the transitional $N = 58$ ^{99}Nb nucleus has a much lower moment of inertia than in the neighboring $N = 60$ and 62 isotopes; this probably indicates a smaller quadrupole deformation, although the effect of pairing correlations cannot be excluded. The almost linear dependence of excitation energy on $I(I+1)$ for the negative-parity decay sequence in ^{99}Nb (Fig. 14), built on the level at $E_x = 631$ keV and with a J^π value of $5/2^-$, provides evidence of a deformed structure; this is the first evidence of a deformed rotational sequence in $N = 58$ ^{99}Nb. Further, the observation of this deformed rotational sequence in ^{99}Nb, in which the decay sequence based on the $9/2^+$ oblate ground state [66] has quite different characteristics, provides the first experimental evidence for the existence of shape coexistence in ^{99}Nb.

Figure 15 shows the experimental signature splitting for the $5/2^+[422]$ bands of ^{101,103}Nb and the $5/2^-[303]$ bands of ^{99,101,103}Nb; the level scheme of ^{99}Nb was based on the present work, while those for ^{101}Nb and ^{103}Nb were based on the works of Hwang *et al.* [64] and Luo *et al.* [9] and of Hwang *et al.* [64] and Hua *et al.* [65], respectively. The $5/2^+[422]$ band of ^{105}Nb, to which reference will be made later, was also identified by Luo *et al.* [9]. For the positive-parity band based on the $5/2^+[422]$ configuration in ^{101,103}Nb, the signature splitting is large compared to that of the negative-parity bands based on the $5/2^-[303]$ configuration in ^{101}Nb and ^{103}Nb. In an axially symmetric nucleus with quadrupole deformation, high-K rotational sequences are expected to exhibit interleaved states with regular spacings and no signature splitting. For nuclei with triaxial deformation, on the other hand, signature splitting is expected. Signature splitting is also observed as a consequence of mixing with $K = 1/2$ bands and here the splitting will increase with increasing rotational frequency. The observed signature splitting in energies of the $5/2^+[422]$ decay sequence in ^{101,103}Nb has been interpreted to be a result of triaxiality [64]. Comparisons of the results of triaxial-rotor-plus-particle calculations with experiment predict that for the $5/2^+[422]$ bands of ^{101,103,105}Nb the quadrupole deformation parameters ϵ_2 are 0.25, 0.36, and 0.37, respectively, and that the values of the triaxiality parameter γ are -5°, -13°, and -15°, respectively [9]. As expected, ϵ_2 increases in value with

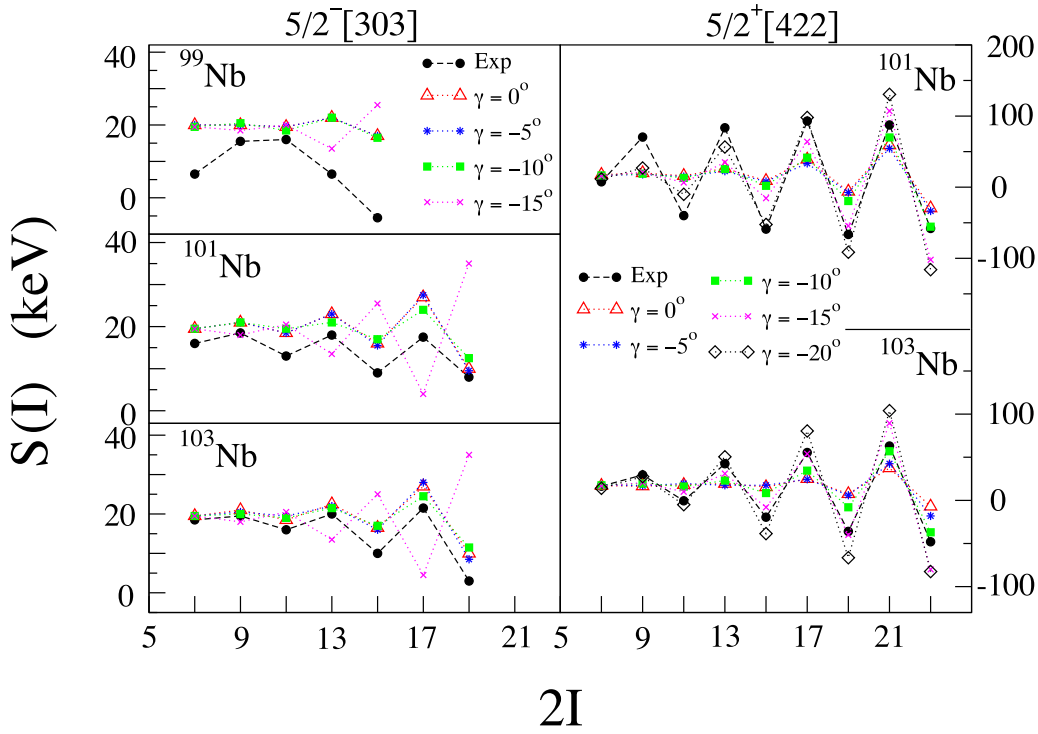

FIG. 16. Comparison of the experimental staggering with the theoretical values based on the particle-plus-rotor model for the $5/2^-[303]$ bands of ^{99}Nb, ^{101}Nb, and ^{103}Nb and for the $5/2^+[422]$ bands of ^{101}Nb and ^{103}Nb. See text for details.

increasing neutron number. For the $5/2^-[303]$ band of ^{101}Nb, a comparison of triaxial-rotor-plus-particle calculations with experiment resulted in a quadrupole deformation parameter of $\epsilon_2 = 0.25$ and a triaxiality parameter of $\gamma = -5^\circ$ [9]. It is noted that, in relation to the signature splitting presented in Fig. 15, the $5/2^-[303]$ band of ^{99}Nb does not show the characteristic behavior corresponding to a stable triaxial shape, nor does it exhibit the behavior expected for $\gamma = 0^\circ$; this will be discussed below.

To understand the role of triaxiality in the $5/2^-[303]$ bands of ^{99,101,103}Nb and in the $5/2^+[422]$ bands of ^{101,103}Nb, calculations were performed using the quasiparticle-plus-rotor model (PRM) with the computer codes GAMPN and ASYRMO [79–81]. This mean-field model, with empirically derived parameters, has been successfully used to interpret the structure of several deformed nuclei in this region. A modified-oscillator potential was used and the particle-plus-triaxial-rotor Hamiltonian was diagonalized in the strong-coupling basis, with the single-particle matrix elements expressed in the deformed scheme, as described in Ref. [81]. Standard empirical values for the μ and κ strength parameters of the $l{\cdot}s$ and $l{\cdot}l$ terms were used [82]. Pairing correlations were taken into account by a standard BCS approximation, using values of $G_0 = 22.0$ MeV and $G_1 = 8.0$ MeV. The Fermi surface and pairing gap Δ are then calculated by the code. Input parameters to the model are A, Z, and the deformations (ε_2, ε_4, ε_6) and γ. The deformation parameters ε_2 and γ were varied in the range $\varepsilon_2 = 0.10 - 0.30$ and $\gamma = 0^\circ - -20^\circ$. All higher order deformations were set to zero. Seven quasiparticle states around the Fermi surface were used in the coupling to the rotor core. The computer code used the hydrodynamical moments of inertia [80,83,84]. The moments of inertia were normalized through the use of an effective core 2^+ energy, which is not directly related to the energy of the core 2^+ state; it is, in fact, a scaling factor which has been fitted to the excitation energies of the odd nucleus. Since $E(2^+)$ is a scaling factor, its variation alone cannot achieve a good energy fit.

Figure 16 shows the experimental signature splitting for the $5/2^-[303]$ bands of ^{99,101,103}Nb and for the $5/2^+[422]$ bands of ^{101,103}Nb. The signature splitting function $S(I)$ used in the figure is defined as [85]:

$$S(I) = \frac{E(I+1) + E(I-1) - 2E(I)}{2}.$$

For the $5/2^+[422]$ band of ^{101}Nb, there is no good agreement between experiment and the results of PRM calculations across the whole spin range with a single value of γ; the higher spins correspond to a γ value of about -15°, while the lower spins correspond to a γ value of about -20°; these conclusions are in agreement with those of Luo *et al.* [9]. For ^{103}Nb, the higher spin members of the $5/2^+[422]$ band have a reasonably good fit with a γ value of -10°, while the lower spin members have a better fit with a γ value of -20°; the conclusion of a similar analysis [9] was that a γ value of -15° corresponded to the best fit across the available spin range. These conclusions may indicate a degree of γ softness for the $5/2^+[422]$ band in ^{101}Nb and ^{101}Nb. For the $5/2^-[303]$ bands of ^{101}Nb and ^{103}Nb, the predicted staggering agrees reasonably well with experiment, but it does not change

significantly for calculations corresponding to γ values of 0°, −5° and −10°, and consequently there is a large uncertainty in the determination of a γ value. For calculations which used $\gamma = -15°$, on the other hand, the phase of the splitting is in disagreement with experiment; signature inversion is predicted. Good fits to the lower-lying energy levels of the $5/2^-[303]$ bands of ^{101}Nb and ^{103}Nb were obtained with an ϵ_2 value of 0.25. It is noted again that for the $5/2^-[303]$ band of ^{101}Nb, an earlier comparison of PRM calculations with experiment yielded an ϵ_2 value of 0.25 [9], in agreement with the present work. A comparison of theory with experiment for ^{99}Nb is poor, see Fig. 16; as noted above, the behavior of the experimental values of $S(I)$ as a function of $2I$ shows neither the characteristic zigzag indicative of triaxiality nor a constant value of $S(I)$, independent of I, which would indicate no triaxiality. This will be discussed below.

D. Cranking calculations for ^{99}Nb

As noted earlier, based on its measured quadrupole moment $[Q_s = -0.42(14)b]$ [66], the ground state of ^{99}Nb ($N = 58$) is expected to be weakly oblate. The relative ordering of the positive-parity levels at low excitation, namely $9/2^+$, $7/2^+$, $5/2^+, \ldots$, in order of increasing energy, see Fig. 7, also attests to the underlying oblate deformation. Here cranking calculations have been performed using the UC code [19] with standard Nilsson parameters. The conclusions of the calculations are that the $9/2^+$ ground state is triaxial (Fig. 17), tending to oblate ($\epsilon_2 = 0.18$, $\gamma = -33°$). A transition to a more deformed prolate shape is indicated beyond $I^\pi = 17/2^+$ ($\epsilon_2 = 0.25$, $\gamma = 0°$), as seen in Fig. 17. Similar behavior is evident in the $N = 58$ isotone, ^{98}Zr, where the analogous 4^+ state in the prolate sequence is yrast [86–88]. The calculations suggest that the prolate shape in ^{99}Nb persists until $I^\pi = 37/2^+$, beyond which a gradual change to a noncollective oblate shape ($\epsilon_2 = 0.19$, $\gamma = +40°$) is visible at $I^\pi = 49/2^+$ (Fig. 17). In the positive-parity band structure built on the $9/2^+$ state, the $\pi g_{9/2}$ crossing is blocked. However, the $\nu h_{11/2}$ band crossing is expected to occur around $\hbar\omega = 0.37$ MeV (Routhian labeled $1/2^-[550]$ in Fig. 18). In the work described here, the decay sequence has been observed to $J^\pi = (29/2^+)$, see Fig. 7. Although the experimental data in ^{99}Nb have not been extended to a sufficiently high angular momentum to observe this crossing, a discontinuity has been observed close to this frequency in the prolate sequence in the ^{98}Zr isotone [86]. Confirmation of the band crossing in ^{99}Nb would, of course, also be of interest.

Similar cranking calculations have also been performed here for the decay sequence based on the $5/2^-[303]$ Nilsson configuration. Figure 19 presents the results for spin values of 5/2, 13/2, and 21/2. The minimum in the potential-energy surface for the $5/2^-$ band head corresponds to $\epsilon_2 = 0.22$ and triaxiality parameter $\gamma = -21°$. For the $13/2^-$ and $21/2^-$ states, the corresponding deformation parameters are $\epsilon_2 = 0.22$, $\gamma = +19°$ and $\epsilon_2 = 0.20$, $\gamma = +10°$, respectively. The predicted rapid variation of triaxiality, including changes in sign, over the observed spin region of the band makes a

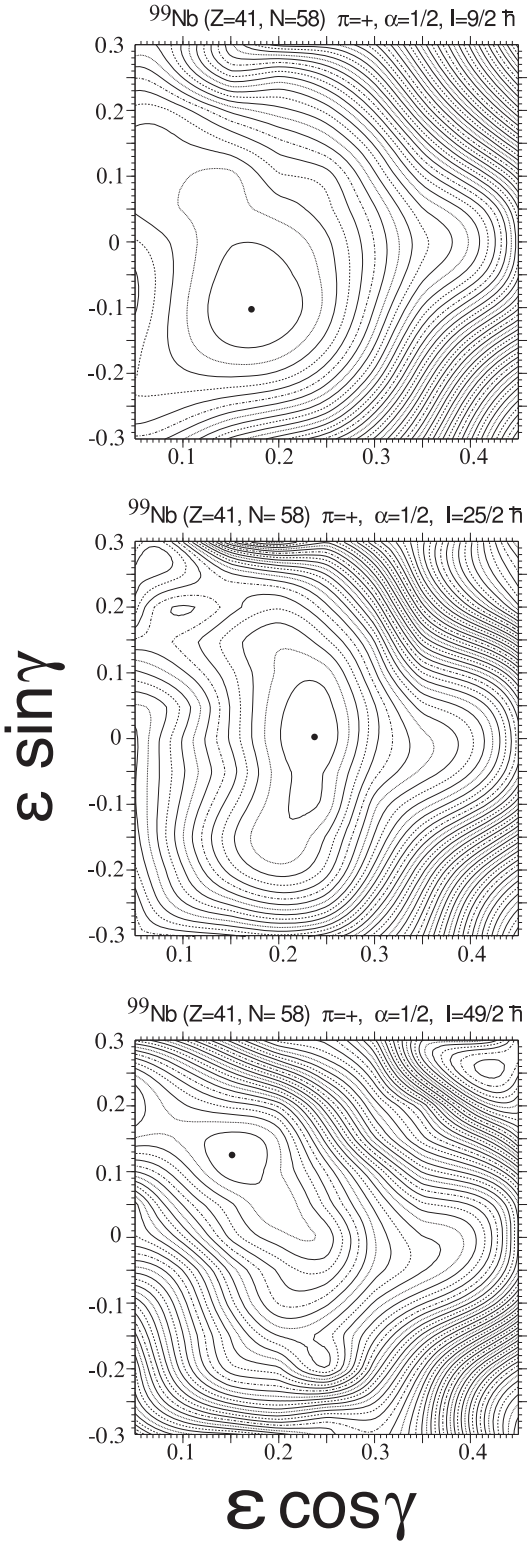

FIG. 17. Total-Energy-Surface plots for the yrast, positive-parity states in ^{99}Nb from the Ultimate Cranker code [19]. The following energy minima are evident: $I^\pi = 9/2^+$: $\epsilon_2 = 0.18$, $\gamma = -30°$; $I^\pi = 25/2^+$: $\epsilon_2 = 0.25$, $\gamma = 0°$; and $I^\pi = 49/2^+$: $\epsilon_2 = 0.19$, $\gamma = +40°$. The spacing between adjacent contours is 200 keV. See text for further details.

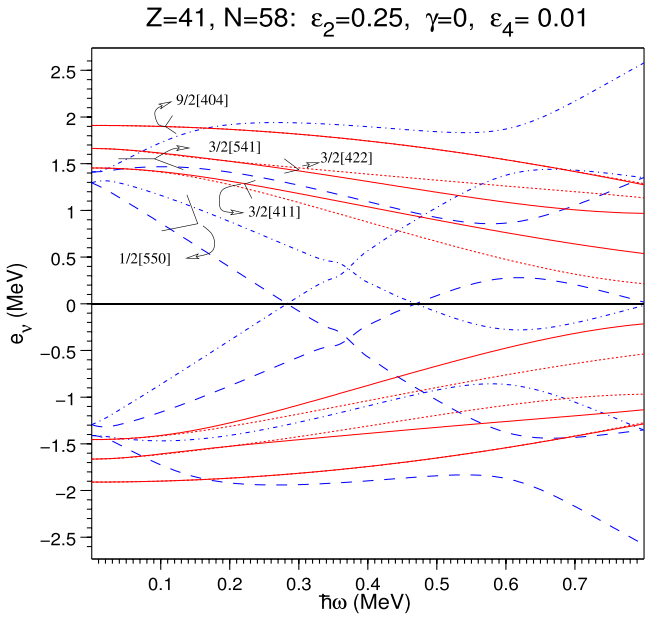

FIG. 18. Quasiparticle Routhian diagram for neutrons. The deformation parameters used in the calculation are indicated in the figure. Parity and signature of the states are as follows: solid: $(+, +1/2)$; dotted: $(+, -1/2)$; dashed-dotted: $(-, +1/2)$ dashed: $(-, -1/2)$.

comparison of experimental data with the results of particle rotor model calculations, see Fig. 16, meaningless; PRM calculations assume a constant value of γ for all band members and this is not the case for the the $5/2^-[303]$ band of ^{99}Nb. On the other hand, the cranking calculations do predict a reasonably constant value of ϵ_2 over the spin range encompassed by the level scheme presented here. The value of ϵ_2, 0.22, for the $5/2^-[303]$ band of ^{99}Nb (see Fig. 19) is comparable to the values for ^{101}Nb and ^{103}Nb which resulted from the PRM calculations discussed above, namely 0.25. In conclusion, the results of the above calculations support the earlier experimental evidence for shape coexistence in the $N = 58$ nucleus ^{99}Nb.

IV. CONCLUSIONS

In the present work, neutron-rich Nb isotopes were populated in binary grazing and fusion-fission reactions. The PRISMA magnetic spectrometer, in conjunction with the CLARA Ge detector array at the INFN Legnaro National Laboratory, were used to identify the isotopes $^{96-99}$Nb and their associated deexcitation γ rays. Relative intensity measurements of the observed γ rays together with the analysis of GASP triples γ-ray coincidence data enabled the construction of level schemes of ^{96,97,99}Nb up to medium spin. It was not possible to construct a level scheme for ^{98}Nb. The level structures of ^{96}Nb and ^{97}Nb are in agreement with the results of earlier experiments. Crucially, in contrast with earlier published studies of the high-spin spectroscopy of ^{96}Nb and ^{97}Nb,

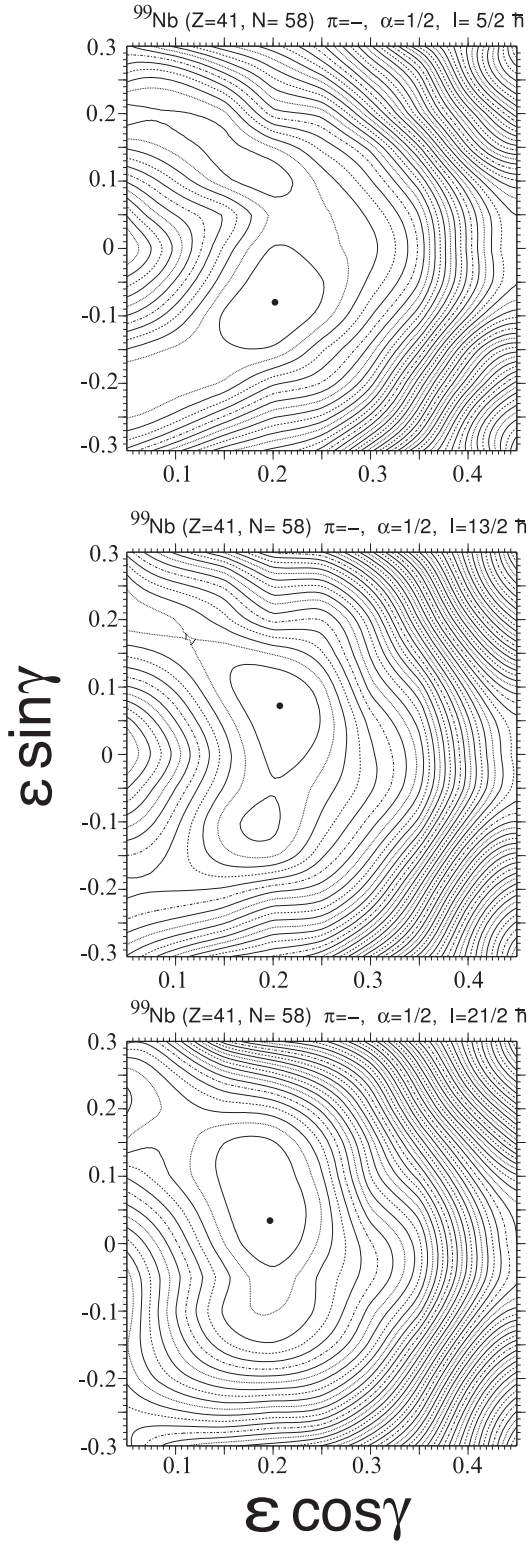

FIG. 19. Total-Energy-Surface plots for the $5/2^-[303]$ decay sequence of ^{99}Nb calculated with the Ultimate Cranker code [19]. The following energy minima are evident: $I^\pi = 5/2^-$: $\epsilon_2 = 0.22$, $\gamma = -21°$; $I^\pi = 13/2^-$: $\epsilon_2 = 0.22$, $\gamma = +19°$; and $I^\pi = 21/2^-$: $\epsilon_2 = 0.20$, $\gamma = +10°$. The spacing between adjacent contours is 200 keV. See text for further details.

the present work provides an unambiguous association of the observed γ rays with the A and Z of the excited nucleus. Two hitherto unobserved decay sequences have been observed in ^{99}Nb; tentative J^{π} values have been assigned on the basis of the systematic behavior of known states in neighboring nuclei. The level structures of ^{96}Nb, ^{97}Nb, and ^{99}Nb can be satisfactorily described within the framework of shell-model calculations; level schemes corresponding to the use of three different shell-model residual interactions were investigated. A previously unobserved deformed band in ^{99}Nb with Nilsson quantum numbers $5/2^{-}[303]$ was populated to spin $(17/2^{-})$; similar rotational sequences have previously been observed in ^{101}Nb and ^{103}Nb but not in the lighter isotopes of niobium. The results of particle-rotor calculations, successful in reproducing the experimental signature splitting of the $5/2^{-}[303]$ band in ^{101}Nb and ^{103}Nb, have been unable to reproduce the experimental data in ^{99}Nb. The results of TRS calculations indicate that, for the $5/2^{-}[303]$ band of ^{99}Nb, the value of the triaxiality parameter γ with increasing angular momentum is not constant either in magnitude or in sign; this offers an explanation of the inability of PRM calculations to reproduce the observed experimental data. It is known that the $9/2^{+}$ ground state of ^{99}Nb is oblate; in the present work a decay sequence build on the ground state has been observed to $J^{\pi} = (29/2^{+})$. Experimentally, the measurement of an oblate shape for the $9/2^{+}$ ground state together with the almost-linear dependence of excitation energy with $I(I+1)$ for the decay sequence based on the $5/2^{-}$ excited state at an excitation energy of 631 keV provide evidence for the first reported observation of two coexisting shapes in the $N = 58$ nucleus, ^{99}Nb; this conclusion is supported by the results of cranking calculations.

ACKNOWLEDGMENTS

The authors thank I. Ragnarsson for very helpful discussions in relation to the particle rotor calculations performed here. This work was supported by the UK Science and Technology Facilities Council (STFC) under Grants No. ST/V001124/1 (UWS) and No. ST/P005101/1 (UWS). In addition, the work was supported by the PN 23 21 01 05 contract sponsored by the Romanian Ministry of Research, Innovation, and Digitalisation and by the IOSIN funds for research infrastructures of Romanian national interest. Finally, the contribution of the accelerator and target-fabrication staff at the INFN Legnaro National Laboratory is gratefully acknowledged.

[1] P. E. Garrett, M. Zielińska, and E. Clément, Prog. Part. Nucl. Phys. **124**, 103931 (2022).
[2] E. Cheifetz, R. C. Jared, S. G. Thompson, and J. B. Wilhelmy, Phys. Rev. Lett. **25**, 38 (1970).
[3] H. Ohm, G. Lhersonneau, K. Sistemich, B. Pfeiffer, and K.-L. Kratz, Z. Phys. A **327**, 483 (1987).
[4] H. Ohm, M. Liang, G. Molnár, and K. Sistemich, Z. Phys. A **334**, 519 (1989).
[5] H. Mach, M. Moszyński, R. L. Gill, F. K. Wohn, J. A. Winger, J. C. Hill, G. Molnár, and K. Sistemich, Phys. Lett. B **230**, 21 (1989).
[6] M. Liang, H. Ohm, B. De Sutter, K. Sistemich, B. Fazekas, and G. Molnär, Z. Phys. A **340**, 223 (1991).
[7] J. H. Hamilton, A. V. Ramayya, S. J. Zhu, G. M. Ter-Akopian, Yu. T. Oganessian, J. D. Cole, J. O. Rasmussen, and M. A. Stoyer, Prog. Part. Nucl. Phys. **35**, 635 (1995).
[8] H. Hua, C. Y. Wu, D. Cline, A. B. Hayes, R. Teng, R. M. Clark, P. Fallon, A. Goergen, A. O. Macchiavelli, and K. Vetter, Phys. Rev. C **69**, 014317 (2004).
[9] Y. X. Luo, J. O. Rasmussen, I. Stefanescu, A. Gelberg, J. H. Hamilton, A. V. Ramayya, J. K. Hwang, S. J. Zhu, P. M. Gore, D. Fong, E. F. Jones, S. C. Wu, I. Y. Lee, T. N. Ginter, W. C. Ma, G. M. Ter-Akopian, A. V. Daniel, M. A. Stoyer, and R. Donangelo, J. Phys. G: Nucl. Part. Phys. **31**, 1303 (2005).
[10] L. Esser, U. Neuneyer, R. F. Casten, and P. von Brentano, Phys. Rev. C **55**, 206 (1997).
[11] N. Fotiades, J. A. Cizewski, R. Krücken, R. M. Clark, P. Fallon, I. Y. Lee, A. O. Macchiavelli, J. A. Becker, and W. Younes, Phys. Rev. C **82**, 044306 (2010).
[12] P. F. Cloessner, W. Stöffl, R. K. Sheline, and R. G. Lanier, Phys. Rev. C **29**, 657 (1984).
[13] D. Abriola and A. A. Sonzogni, Nucl. Data Sheets **109**, 2501 (2008).
[14] A. Siivola and G. Graeffe, Nucl. Phys. A **109**, 369 (1968).
[15] H. A. Selič, G. Sadler, T. A. Khan, W.-D. Lauppe, H. Lawin, K. Sistemich, E. Monnand, J. Blachot, J. P. Bocquet, and F. Schussler, Z. Phys. A **289**, 197 (1979).
[16] N. Nica, Nucl. Data Sheets **111**, 525 (2010).
[17] E. Browne and J. K. Tuli, Nucl. Data Sheets **145**, 25 (2017).
[18] V. Kumar, R. Chapman, A. Hodsdon, X. Liang, J. F. Smith, K. M. Spohr, D. A. Torres, P. Wady, Z. Wang, D. O'Donne, J. Ollier, M. Labiche, G. Pollarolo, S. Aydin, D. Bazzacco, E. Farnea, A. Gottardo, T. Kroell, S. Lunardi, D. Mengoni, R. Mărginean, F. Recchia, C. A. Ur, G. de Angelis, A. Gadea, B. Guiot, N. Mărginean, P. Mason, T. Martinez, D. R. Napoli, R. Orlandi, F. Della Vedova, J. J. Valiente-Dobón, S. J. Freeman, A. G. Smith, G. Jones, N. J. Thompson, and T. Faul, LNL Ann. Rep. **15**, 15 (2008).
[19] T. Bengtsson, Nucl. Phys. A **512**, 124 (1990).
[20] D. Bazzacco (The GASP Collaboration), *Proceedings of the Conference on Nuclear Structure at High Angular Momentum*, Report No. AECL 10613, Vol. 2, Ottawa, Chalk River, Canada, 1992, p. 376.
[21] C. Rossi Alvarez, Nucl. Phys. News **3**, 10 (1993).
[22] A. M. Stefanini, L. Corradi, G. Maron, A. Pisent, M. Trotta, A. M. Vinodkumar, S. Beghini, G. Montagnoli, F. Scarlassara, G. F. Segato, A. De Rosa, G. Inglima, D. Pierroutsakou, M. Romoli, M. Sandoli, G. Pollarolo, and A. Latina, Nucl. Phys. A **701**, 217 (2002).
[23] S. Szilner, C. A. Ur, L. Corradi, N. Mărginean, G. Pollarolo, A. M. Stefanini, S. Beghini, B. R. Behera, E. Fioretto, A. Gadea, B. Guiot, A. Latina, P. Mason, G. Montagnoli, F. Scarlassara, M. Trotta, G. de Angelis, F. Della Vedova, E. Farnea, F. Haas, S. Lenzi, S. Lunardi, R. Mărginean, R. Menegazzo, D. R. Napoli, M. Nespolo, I. V. Pokrovsky, F. Recchia, M. Romoli, M.-D. Salsac, N. Soić, and J. J. Valiente-Dobón, Phys. Rev. C **76**, 024604 (2007).

[24] A. Gadea *et al.* (The EUROBALL and PRISMA-2 Collaborations), Eur. Phys. J. A **20**, 193 (2003).

[25] A. Latina, Study of heavy-ion reactions with the magnetic spectrometer PRISMA, Ph.D. thesis, Università Degli Studi di Torino, 2004.

[26] G. Montagnoli, A. M. Stefaninib, M. Trottac, S. Beghinia, M. Bettinia, F. Scarlassaraa, V. Schiavona, L. Corradib, B. R. Beherab, E. Fiorettob, A. Gadeab, A. Latinab, S. Szilnerb, L. Doná, M. Rigatob, N. A. Kondratieve, A. Yu. Chizhove, G. Kniajevae, E. M. Kozuline, I. V. Pokrovskiye, V. M. Voskressenskye, and D. Ackermannf, Nucl. Instrum. Methods A **547**, 455 (2005).

[27] S. Beghini, L. Corradi, E. Fioretto, A. Gadea, A. Latina, G. Montagnoli, F. Scarlassara, A. M. Stefanini, S. Szilner, M. Trotta, and A. M. Vinodkumar, Nucl. Instrum. Methods A **551**, 364 (2005).

[28] D. Bazzaco (private communication).

[29] D. C. Radford, Nucl. Instrum. Methods A **361**, 297 (1995).

[30] B. D. Kern, T. Fényes, A. Krasznahorkay, Zs. Dombrádi, S. Brant, and V. Paar, Nucl. Phys. A **430**, 301 (1984).

[31] J. R. Comfort, J. V. Maher, G. C. Morrison, and J. P. Schiffer, Phys. Rev. Lett. **25**, 383 (1970).

[32] M. S. Zisman and B. G. Harvey, Phys. Rev. C **5**, 1031 (1972).

[33] J. H. Thies, P. Puppe, T. Adachi, M. Dozono, H. Ejiri, D. Frekers, H. Fujita, Y. Fujita, M. Fujiwara, E.-W. Grewe, K. Hatanaka, P. Heinrichs, D. Ishikawa, N. T. Khai, A. Lennarz, H. Matsubara, H. Okamura, Y. Y. Oo, T. Ruhe, K. Suda *et al.*, Phys. Rev. C **86**, 054323 (2012).

[34] S. Cochavi and D. B. Fossan, Phys. Rev. C **5**, 164 (1972).

[35] L. R. Medsker, Phys. Rev. C **8**, 1906 (1973).

[36] P. K. Bindal, D. H. Youngblood, and R. L. Kozub, Phys. Rev. C **10**, 729 (1974).

[37] E. R. Flynn, R. E. Brown, F. Ajzenberg-Selove, and J. A. Cizewski, Phys. Rev. C **28**, 575 (1983).

[38] G. Lhersonneau, J. Suhonen, P. Dendooven, A. Honkanen, M. Huhta, P. Jones, R. Julin, S. Juutinen, M. Oinonen, H. Penttilä, J. R. Persson, K. Peräjärvi, A. Savelius, J. C. Wang, J. Äystö, S. Brant, V. Paar, and D. Vretenar, Phys. Rev. C **57**, 2974 (1998).

[39] D. Bucurescu, Zs. Podolyák, G. de Angelis, Y. H. Zhang, G. Căta-Danil, I. Căta-Danil, M. Ivaşcu, N. Mărginean, R. Mărginean, L. C. Mihăilescu, G. A. Suliman, P. H. Regan, W. Gelletly, S. D. Langdown, J. J. Valiente Dobón, D. Bazzacco, S. Lunardi, C. A. Ur, M. Axiotis, A. Gadea, E. Farnea, M. Ionescu-Bujor, A. Iordăchescu, T. Kröll, T. Martinez, P. G. Bizzetti, R. Broda, N. H. Medina, B. Quintana, and B. Rubio, Phys. Rev. C **71**, 034315 (2005).

[40] N. Fotiades, J. A. Cizewski, J. A. Becker, L. A. Bernstein, D. P. McNabb, W. Younes, R. M. Clark, P. Fallon, I. Y. Lee, A. O. Macchiavelli, A. Holt, and M. Hjorth-Jensen, Phys. Rev. C **65**, 044303 (2002).

[41] D. Pantelica, I. Gh. Stefan, N. Nica, M.-G. Porquet, G. Duchêne, A. Astier, S. Courtin, I. Deloncle, F. Hoellinger, A. Bauchet, N. Buforn, L. Donadille, O. Dorvaux, J. Duprat, B. J. P. Gall, C. Gautherin, T. Kutsarova, S. Lalkovski, R. Lucas, M. Meyer, A. Minkova, A. Prévost *et al.*, Phys. Rev. C **72**, 024304 (2005).

[42] C. Y. Wu, H. Hua, D. Cline, A. B. Hayes, R. Teng, R. M. Clark, P. Fallon, A. Goergen, A. O. Macchiavelli, and K. Vetter, Phys. Rev. C **70**, 064312 (2004).

[43] L. Bettermann, J.-M. Régis, T. Materna, J. Jolie, U. Köster, K. Moschner, and D. Radeck, Phys. Rev. C **82**, 044310 (2010).

[44] C. M. Lederer, J. M. Jaklevic, and J. M. Hollander, Nucl. Phys. A **169**, 449 (1971).

[45] J. M. Chatterjee, M. Saha-Sarkar, S. Bhattacharya, P. Banerjee, S. Sarkar, R. P. Singh, S. Murulithar, and R. K. Bhowmik, Nucl. Phys. A **678**, 367 (2000).

[46] S. Lalkovski, S. Ilieva, A. Minkova, N. Minkov, T. Kutsarova, A. Lopez-Martens, A. Korichi, H. Hübel, A. Görgen, A. Jansen, G. Schönwasser, B. Herskind, M. Bergström, and Z. Podolyák, Phys. Rev. C **75**, 014314 (2007).

[47] D. Abriola and A. A. Sonzogni, Nucl. Data Sheets **107**, 2423 (2006).

[48] J. Chen and B. Singh, Nucl. Data Sheets **164**, 1 (2020).

[49] B. Singh and J. Chen, Nucl. Data Sheets **172**, 1 (2021).

[50] S. K. Basu, G. Mukherjee, and A. A. Sonzogni, Nucl. Data Sheets **111**, 2555 (2010).

[51] G. Lhersonneau, P. A. Butler, J. F. C. Cocks, A. Honkanen, M. Huhta, P. M. Jones, A. Jokinen, R. Julin, S. Juutinen, A. Lampinen, D. Müller, E. Mäkelä, M. Oinonen, J. M. Parmonen, M. Piiparinen, A. Savelius, J. F. Smith, S. Törmänen, A. Virtanen, and J. Äystö, Nucl. Instrum. Methods A **373**, 415 (1996).

[52] F. Hoellinger, N. Schulz, S. Courtin, B. J. P. Gall, M.-G. Porquet, I. Deloncle, A. Wilson, T. Kutsarova, A. Minkova, J. Duprat, H. Sergolle, C. Gautherin, and R. Lucas, Eur. Phys. J. A **4**, 319 (1999).

[53] J. Blachot, Nucl. Data Sheets **45**, 701 (1985).

[54] D. De Frenne, Nucl. Data Sheets **110**, 2081 (2009).

[55] D. E. Miracle and B. D. Kern, Nucl. Phys. A **320**, 353 (1979).

[56] N. Mărginean, D. Bucurescu, G. Căta-Danil, I. Căta-Danil, M. Ivaşcu, and C. A. Ur, Phys. Rev. C **62**, 034309 (2000).

[57] B. A. Brown and D. B. Fossan, Phys. Rev. C **15**, 2044 (1977).

[58] C. M. Baglin, Nucl. Data Sheets **113**, 2187 (2012).

[59] S. S. Ghugre, B. Kharraja, U. Garg, R. V. F. Janssens, M. P. Carpenter, B. Crowell, T. L. Khoo, T. Lauritsen, D. Nisius, W. Reviol, W. F. Mueller, L. L. Riedinger, and R. Kaczarowski, Phys. Rev. C **61**, 024302 (1999).

[60] D. Bucurescu, G. Căta-Danil, I. Căta-Danil, M. Ivascu, N. Mărginean, C. Rusu, L. Stroe, C. A. Ur, A. Gizon, J. Gizon, B. Nyakó, J. Timár, L. Zolnai, A. J. Boston, D. T. Joss, E. S. Paul, A. T. Semple, and C. M. Parry, Eur. Phys. J. A **10**, 255 (2001).

[61] A. M. Bizzeti-Sona, P. Blasi, A. A. Stefanini, and A. J. Kreiner, Phys. Rev. C **36**, 2330 (1987).

[62] D. Huai-Bo, Z. Sheng-Jiang, W. Jian-Guo, G. Long, X. Qiang, X. Zhi-Gang, Y. Eing-Yee, Z. Ming, Z. Li-Hua, W. Xiao-Guang, L. Ying, H. Chuang-Ye, W. Lie-Lin, P. Bo, and L. Guang-Sheng, Chin. Phys. Lett. **27**, 072501 (2010).

[63] H. Ohm, M. Liang, U. Paffrath, B. De Sutter, K. Sistemich, A.-M. Schmitt, N. Kaffrell, N. Trautmann, T. Seo, K. Shizuma, G. Molnár, K. Kawade, and R. A. Meyer, Z. Phys. A **340**, 5 (1991).

[64] J. K. Hwang, A. V. Ramayya, J. Gilat, J. H. Hamilton, L. K. Peker, J. O. Rasmussen, J. Kormicki, T. N. Ginter, B. R. S. Babu, C. J. Beyer, E. F. Jones, R. Donangelo, S. J. Zhu, H. C. Griffin, G. M. Ter Akopian, Yu. T. Oganessian, A. V. Daniel, W. C. Ma, P. G. Varmette, J. D. Cole, R. Aryaeinejad, M. W. Drigert *et al.*, Phys. Rev. C **58**, 3252 (1998).

[65] H. Hua, C. Y. Wu, D. Cline, A. B. Hayes, R. Teng, R. M. Clark, P. Fallon, A. O. Macchiavelli, and K. Vetter, Phys. Rev. C **65**, 064325 (2002).

[66] B. Cheal, K. Baczynska, J. Billowes, P. Campbell, F. C. Charlwood, T. Eronen, D. H. Forest, A. Jokinen, T. Kessler, I. D.

Moore, M. Reponen, S. Rothe, M. Rüffer, A. Saastamoinen, G. Tungate, and J. Äystö, Phys. Rev. Lett. **102**, 222501 (2009).
[67] S. Lalkovski, J. Timar, and Z. Elekes, Nucl. Data Sheets **161-162**, 1 (2019).
[68] B. M. Preedom, E. Newman, and J. C. Hiebert, Phys. Rev. **166**, 1156 (1968).
[69] B. A. Brown, W. D. M. Rae, E. McDonald, and M. Horoi, NUSHELLX@MSU, https://people.nscl.msu.edu/~brown/resources/resources.html.
[70] D. H. Gloeckner, Nucl. Phys. A **253**, 301 (1975).
[71] H. Mach, E. K. Warburton, R. L. Gill, R. F. Casten, J. A. Becker, B. A. Brown, and J. A. Winger, Phys. Rev. C **41**, 226 (1990).
[72] M. Hjorth-Jensen, T. T. S. Kuo, and E. Osnes, Phys. Rep. **261**, 125 (1995).
[73] B. A. Brown, A. Etchegoyen, W. D. M. Rae, and N. S. Godwin, MSU-NSCL Report No. 524, 1985 (unpublished).
[74] D. H. Gloeckner and F. J. D. Serduke, Nucl. Phys. A **220**, 477 (1974).
[75] R. Machleidt, Phys. Rev. C **63**, 024001 (2001).
[76] R. Machleidt, K. Holinde, and C. Elster, Phys. Rep. **149**, 1 (1987).
[77] R. Machleidt, Adv. Nucl. Phys. **19**, 189 (1989).
[78] T. Konstantinopoulos, P. Petkov, A. Goasduff, T. Arici, A. Astier, L. Atanasova, M. Axiotis, D. Bonatsos, P. Detistov, A. Dewald, M. J. Eller, V. Foteinou, A. Gargano, G. Georgiev, K. Gladnishki, A. Gottardo, S. Harissopulos, H. Hess, S. Kaim, D. Kocheva *et al.*, Phys. Rev. C **95**, 014309 (2017).
[79] I. Ragnarsson and P. Semmes, University of Lund (1991-1999) (unpublished).
[80] I. Ragnarsson and P. B. Semmes, Hyperfine Interact. **43**, 423 (1988).
[81] S. E. Larsson, G. Leander, and I. Ragnarsson, Nucl. Phys. A **307**, 189 (1978).
[82] T. Bengtsson and I. Ragnarsson, Nucl. Phys. A **436**, 14 (1985).
[83] S. G. Nilsson and I. Ragnarsson, *Shapes and Shells in Nuclear Structure* (Cambridge University Press, Cambridge, UK, 1995).
[84] A. Bohr and B. Mottelson, *Nuclear Structure* (Benjamin, New York, 1975), Vol. 2.
[85] J. A. Pinston, W. Urban, Ch. Droste, T. Rzaca-Urban, J. Genevey, G. Simpson, J. L. Durell, A. G. Smith, B. J. Varley, and I. Ahmad, Phys. Rev. C **74**, 064304 (2006).
[86] W. Urban, J. L. Durell, A. G. Smith, W. R. Phillips, M. A. Jones, B. J. Varley, T. Rzaca-Urban, I. Ahmad, L. R. Morss, M. Bentaleb, and N. Schulz, Nucl. Phys. A **689**, 605 (2001).
[87] W. Witt, V. Werner, N. Pietralla, M. Albers, A. D. Ayangeakaa, B. Bucher, M. P. Carpenter, D. Cline, H. M. David, A. Hayes, C. Hoffman, R. V. F. Janssens, B. P. Kay, F. G. Kondev, W. Korten, T. Lauritsen, O. Möller, G. Rainovski, G. Savard, D. Seweryniak *et al.*, Phys. Rev. C **98**, 041302(R) (2018).
[88] P. Singh, W. Korten, T. W. Hagen, A. Görgen, L. Grente, M.-D. Salsac, F. Farget, E. Clément, G. de France, T. Braunroth, B. Bruyneel, I. Celikovic, O. Delaune, A. Dewald, A. Dijon, J.-P. Delaroche, M. Girod, M. Hackstein, B. Jacquot, J. Libert, and C. Theisen, Phys. Rev. Lett. **121**, 192501 (2018).